A Novel Approach to Experimental Studies of Mineral Dissolution Kinetics

Annual Technical Progress Report

Performance Period **September 1, 2005 – August 31, 2006**

CHEN ZHU
Indiana University

WILLIAM E. SEYFRIED
University of Minnesota

November 29, 2006

Award Number **DE-FG26-04NT42125**

Department of Geological Sciences, Indiana University, Bloomington, IN 47405. Phone: (812) 855-1884, FAX: (812) 855-7899,
e-mail: chenzhu@indiana.edu

Disclaimer

Abstract

Currently, DOE is conducting pilot CO_2 injection tests to evaluate the concept of geological sequestration. One strategy that potentially enhances CO_2 solubility and reduces the risk of CO_2 leak back to the surface is dissolution of indigenous minerals in the geological formation and precipitation of secondary carbonate phases, which increases the brine pH and immobilizes CO_2. Clearly, the rates at which these dissolution and precipitation reactions occur directly determine the efficiency of this strategy. However, one of the fundamental problems in modern geochemistry is the persistent two to five orders of magnitude discrepancy between laboratory-measured and field derived feldspar dissolution rates. To date, there is no real guidance as to how to predict silicate reaction rates for use in quantitative models. Current models for assessment of geological carbon sequestration have generally opted to use laboratory rates, in spite of the dearth of such data for compositionally complex systems, and the persistent disconnect between laboratory and field applications. Therefore, a firm scientific basis for predicting silicate reaction kinetics in CO_2 injected geological formations is urgently needed to assure the reliability of the geochemical models used for the assessments of carbon sequestration strategies.
The funded experimental and theoretical study attempts to resolve this outstanding scientific issue by novel experimental design and theoretical interpretation to measure silicate dissolution rates and iron carbonate precipitation rates at conditions pertinent to geological carbon sequestration.

In the second year of the project, we completed CO_2-Navajo sandstone interaction batch and flow-through experiments and a Navajo sandstone dissolution experiment without the presence of CO_2 at 200 ^oC and 250-300 bars, and initiated dawsonite dissolution and solubility experiments. We also performed additional 5-day experiments at the same conditions as alkali-feldspar dissolution experiments with and without the presence of CO_2 performed in the first year to check the validation of the experiments and analysis. The changes of solution chemistry as dissolution experiments progressed were monitored with on-line sampling of the aqueous phase at the constant temperature and pressure. These data allow calculating overall apparent mineral (feldspars and sandstones) dissolution rates and secondary mineral precipitation rates as a function of saturation states. State-of-the-art atomic resolution transmission electron microscopy (TEM), scanning electron microscopy (SEM), and electron microprobe was used to characterize the products and reactants. Reaction-path geochemical modeling was used to interpret the experimental results of alkali-feldspar dissolution experiments without the presence of CO_2. Two manuscripts are near completion.

Also during the second year, our education goal of graduate student training has been advanced. A Ph. D. student at Indiana University is progressing well in the degree program and has taken geochemical modeling, SEM, and TEM courses, which will facilitate research in the third year. A Ph. D. student at University of Minnesota had graduated. With the success of training of graduate students and excellent experimental data in the second year, we anticipate a more fruitful year in the third year.

Table of Contents

1. Introduction

There has been a great deal of concern over global climate change, and its link to growing atmospheric concentrations of carbon dioxide (CO_2). An ever-increasing amount of scientific evidence suggests that anthropogenic release of CO_2 has led to a rise in global temperatures over the past several hundred years (Crowley, 2000; Bradley, 2001). This "global warming" is a trend that, if unabated, can lead to significant and possibly catastrophic alteration of climate throughout the world.

In order to decrease the impact of CO_2 on global climate, several strategies are under development that will potentially remove CO_2 from the atmosphere or decrease CO_2 emission (Herzog et al., 1997; Doe, 1999). One such strategy that has received a great deal of attention involves the capture of CO_2 from large point sources (such as fossil fuel-fired power plants) and the long-term storage of CO_2 underground. In fact, such a technique is currently in practice in Norway. Statoil's Sleipner plant separates about 2,800 tons of CO_2 from a natural gas stream daily and injects it into a saline aquifer below the North Sea (Hammerstad, 2000).

For geological carbon sequestration programs that inject CO_2 into deep saline formations, the injected CO_2 can react with brine and solid matrix, resulting in an increase of pH and precipitation of carbonates. The rate of this reaction with respect to fluid flow is important to determine the mechanism of trapping, either by hydrodynamics (CO_2 dissolved in slow moving brine or remains to be in a separate liquid phase) or mineral trapping (carbon precipitation). Such processes are currently being evaluated at NETL sponsored pilot test sites in the Frio sandstone in the Texas Gulf Coast (Hovorka et al., 2002), at Statoil's Sliepner project in North Sea (Johnson et al., 2002), and at the Weyburn CO_2-enhanced oil recovery site, Canada (Perkins et al., 2002).

Recently, STRAZISAR et al. (2003) performed one-dimensional transport modeling of CO_2 in the Alberta basin, with the chemical reaction aspect of the model resembling that presented by GUNTER et al. (2000) as a first approximation. The ultimate goal of this modeling effort is to develop reservoir or basin scale models that include flow, mass and heat transport, multi-phases, and chemical reaction processes at field pilot test and CO_2 injection sites. Such a model is valuable for evaluating the suitability of a geological formation as CO_2 storage, optimal injection operations, and monitoring and management of injection operations.

One outcome of this modeling study is the demonstrated importance of mineral reaction kinetics. However, one of the fundamental problems in modern geochemistry is the persistent two to five orders of magnitude discrepancy between laboratory-measured and field derived feldspar dissolution rates (see reviews by Blum and Stillings, 1995; Drever and Clow, 1995; White, 1995). This discrepancy is huge. For example, the laboratory rates indicate that a 0.1 mm feldspar sphere should weather away in ~250 years, whereas the field rates predict a feldspar lifetime of millions of years (calculations followed Lasaga, 1998). Such a large discrepancy illustrates our inability to move forward with the quantitative assessment of mineral trapping as a sequestration strategy. In addition to the geological carbon sequestration program, kinetically controlled reactions, including glauconite dissolution (Gunter et al., 1997), iron carbonate precipitation (Nrc, 2003), and olive and serpentine carbonation (Carey et al., 2003, and reports published by the Albany Research Center), are also important to other carbon sequestration programs.

To date, there is no real guidance as to how to predict *in situ* reaction rates for use in reactive transport models. Models for geological carbon sequestration have generally opted to use laboratory rates (e.g., Gunter et al., 1997; Xu et al., 2003). In general, we know little about the proper rates and rate laws that are applicable to geological systems (Lasaga, 1998). However, a firm scientific basis for predicting reaction kinetics in natural environments is urgently needed to assure the reliability of the geochemical models used for the carbon sequestration program.

The funded research here attempts to resolve this **outstanding scientific issue**. The chemical, physical, and biological processes in the deep geological formation are complex and inter-related. Monitoring subsurface activities is costly. Thus, the results of the funded research represents a necessary step in **reducing cost** associated with geological carbon sequestration by developing mathematical models for evaluating and optimizing the injection program. Over the long-term, geological carbon sequestration will go through performance assessment evaluation processes, and as time progresses, the reaction kinetics problem is likely to occupy a more prominent position. Our results will provide crucial parameters for the performance assessment.

Feldspars (Fig. 1) are the most abundant silicate minerals and comprise over 50% of the volume of the earth's crust. When CO_2 is injected into geological formations, CO_2 will react with silicate minerals in the aquifers (such as in the case of the Frio sandstone, Texas, Weyburn, Canada, and the Sleipner projects mentioned above). The reactions will increase the pH of the brine, resulting in an enhanced solubility of CO_2 in brine, which is a desirable effect because it reduces the chance of CO_2 leakage to the surface.

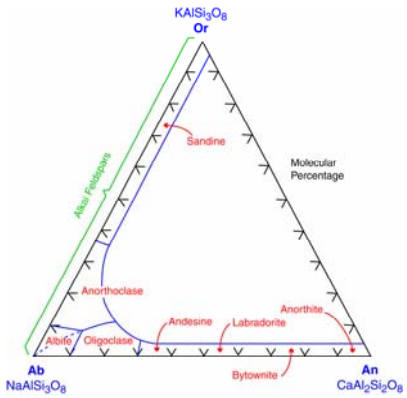

Figure 1. Chemical compositions and nomenclature of feldspars.

Dissolution of feldspars can also release Ca^{2+}, which can form carbonate precipitates. This is the most desired consequence of CO_2 injection because carbonate solids are immobile and are permanently stored in deep geological formations without the risk of seeping back to the surface. As pointed out by the NRC workshop report (Nrc, 2003), this is a natural process of weathering. However, the key to the carbon sequestration program is an understanding of the reaction kinetics and how to accelerate the process.

Another consequence of silicate reaction after CO_2 injection is the change of porosities in the geological formation, which can alter the patterns of fluid flow and cause formation damage. STRAZISAR et al. (2003) again demonstrated that the magnitudes of porosity changes are closely related to the kinetic parameters used in the model.

In addition to the long-term controversy between field and laboratory rates, there is a general lack of experimental data at conditions pertinent to the geological carbon sequestration program. The reactions pertinent to geological carbon sequestration occur in about 50 to 150 ^{o}C, high CO_2 pressure, and in saline brines. Although high CO_2 concentrations might suggest pH lowering and more rapid dissolution of primary aluminosilicates, these conditions may enhance further the stability of clay minerals and carbonate minerals, with attendant effects on the overall reaction rate schemes. Moreover, it is not at all clear from available data whether high CO_2

concentrations in fluids act to catalyze or inhibit mineral dissolution/precipitation processes typical of or likely to be found in geologic terrains impacted by carbon sequestration.

There is a dearth of kinetic data relevant to geological carbon sequestration, and hence the need for experimental measurements.

Furthermore, we want to test experimentally the feasibility of using some unconventional CO_2 storage formations. Red sandstone beds are widespread worldwide and co-injection of SO_2 and CO_2 could reduce ferric iron to ferrous iron and form **iron carbonate** precipitates. One of the major costs of the carbon sequestration program is the capture and purification of CO_2 at point sources. If some impurities in flue gas, such as SO_2, can have beneficial use, it represents a major cost reduction to the program. Although theoretical calculations show great promise for this strategy (Knauss et al., 2002; Palandri and Kharaka, 2003), the redox reactions are dominated by kinetics and little experimental kinetic data are available.

With these goals in mind, we have devised an innovative experimental and theoretical interpretation program to address these urgent and significant outstanding scientific issues facing the carbon sequestration program.

We made progress during the first two years of this 3-year project. During the first year, we accomplished the following:

- We successfully developed a sample preparation method and prepared reactants for experiments. The samples were characterized by electron microprobe, Scanning Electron Microscopy (SEM) and High Resolution Transmission Electron Microscope (TEM), which established a baseline for characterizing the products from experiments.

- We successfully completed three batch type feldspar dissolution experiments and obtained time series solution chemistry data. The products from these experiments are being analyzed (see below).

- We made significant progress on characterization of the reaction products of alkali-feldspars by using SEM, TEM, and XPS.

- We conducted a substantial amount of geochemical modeling work on interpretation of experimental results.

In summary, we met or exceeded the first year milestones. Our objectives for the second year were:

1) Experimental measurements of feldspar dissolution, dawsonite dissolution, and iron carbonate formation at conditions pertinent to the geological carbon sequestration program;
2) Atomic or near atomic scale electron microscopy of the reactants and products to discern the reaction mechanisms;
3) Theoretical and modeling studies to interpret and synthesize experimental data, and development of a strategy to simulate *in situ* reaction kinetics in geological formation.

Both completed and on-going experiments are listed in Table 1. Experiments 1, 2 and 6 were carried out in the first year and experiments 3, 4 and 5 were carried out in the second year. Experiment 7 is still on-going.

Table 1. Summary of Experiments

	Time	Materials	conditions
Exp. 1	Year 1*	Alkali-feldspar from Wards. 35% low albite ($Ca_{0.04}Na_{0.95}K_{0.01}Al_{1.04}Si_{2.96}O_8$), 60% orthoclase ($K_{0.85}Na_{0.15}Al_{1.04}Si_{2.97}O_8$), and 5% of quartz.	200 °C, 300 bars 0.2 M KCl with 0.05 M CO_2, pH 4
Exp. 2	Year 1*	Alkali-feldspar from Wards. 35% low albite ($Ca_{0.04}Na_{0.95}K_{0.01}Al_{1.04}Si_{2.96}O_8$), 60% orthoclase ($K_{0.85}Na_{0.15}Al_{1.04}Si_{2.97}O_8$), and 5% of quartz.	200 °C, 300 bars 0.2 M KCl without CO_2, pH 3
Exp.3	Year 2	Navajo sandstone	200 °C, 300 bars 0.2 M KCl with 0.02 M CO_2, pH 5.5 (in-situ)
Exp. 4	Year 2	Navajo sandstone 2.	200 °C, 300 bars 0.2 M KCl without CO_2, pH 5.5 (in-situ)
Exp. 5	Year 2	Navajo sandstone 3. (flow through reactor)	200 °C, 250 bars 0.2 M KCl without CO_2, pH 3.9 (25 °C)
Exp. 6	Year 1	"K-feldspar" from IU. 30% low albite ($NaAl_{1.04}Si_{2.96}O_8$), 70% microcline ($K_{0.94}Na_{0.06}Al_{1.03}Si_{2.97}O_8$).	200 °C, 300 bars 0.05 M NaCl with 6 mM CO_2, pH 6.1 (in-situ)
Exp. 7	Year 2 (on-going)	Dawsonite precipitation	

*In the second year, we performed additional 5-day alkali-feldspar dissolution experiments under the same conditions as experiments 1 and 2 to check the validation of the experiments and analysis.

2. Executive Summary

Currently, DOE is conducting pilot CO_2 injection tests to evaluate the concept of geological sequestration. One strategy that potentially enhances CO_2 solubility and reduces the risk of CO_2 leak back to the surface is dissolution of indigenous minerals in the geological formation and precipitation of secondary carbonate phases, which increases the brine pH and immobilizes CO_2. Clearly, the rates at which these dissolution and precipitation reactions occur directly determine the efficiency of this strategy. However, one of the fundamental problems in modern geochemistry is the persistent two to five orders of magnitude discrepancy between laboratory-measured and field derived feldspar dissolution rates. To date, there is no real guidance as to how to predict silicate reaction rates for use in quantitative models. Therefore, a firm scientific basis for predicting silicate reaction kinetics in CO_2 injected geological formations is urgently needed to assure the reliability of the geochemical models used for the assessments of carbon sequestration strategies.

This research project addresses this critical and urgent need of the carbon sequestration program. The research program is built upon the PIs' substantial previous work in the field of water-gas-rock interactions, including some work in the carbon sequestration program. Hence, the funded work can be easily integrated with the NETL in-house research, and NETL-sponsored programs of field tests of injecting CO_2 into deep geological formations (Frio sandstone, Sleipner, and Weyburn projects), and mineral carbonation and brine sequestration programs (NETL, Los Alamos, Albany Research Center).

During the second year of this three year project, the following accomplishments have been made:

1. We completed two batch type experiments and one flow through reactor experiment with Navajo sandstones and obtained time series solution chemistry data. An additional batch experiment was initiated with dawsonite. We also performed additional 5-day experiments at the same conditions as alkali-feldspar dissolution experiments with and without the presence of CO_2 performed in the first year to check the validation of the experiments and analysis. The changes of solution chemistry as dissolution experiments progressed were monitored with on-line sampling of the aqueous phase at the constant temperature and pressure. These data allow calculating overall apparent mineral (feldspars and sandstones) dissolution rates and secondary mineral precipitation rates as a function of saturation states. The products from these experiments provide the opportunity to characterize the reacted mineral surfaces.

2. We used SEM, TEM, and XPS to characterize the mineral products. SEM shows that the surfaces of reacted sandstone and feldspar grains are covered with secondary clay particles. TEM study shows that they are sheet silicates. We are making significant progress on using High Resolution TEM to characterize the mineral surfaces.

3. We conducted geochemical modeling work on interpretation of experimental results. We completed the modeling for one experiment, and are continuing the modeling work on other experiments.

In summary, we have largely met or exceeded the milestones during the second year. We anticipate that the third year will be a fruitful year as our graduate students are already trained and results from the second year are ready for interpretation and publication. Overall, our results will help to resolve one of the major outstanding scientific issues facing the carbon sequestration program: the rates of chemical reactions in geological formations. The results will benefit the program by introducing the development of numerical performance assessment models, which will reduce the costs of monitoring and design.

3. Experimental

3.1. Navajo Sandstones Sample Preparation

Reddish Navajo sandstones were collected from N aquifer, Black Mesa, Arizona. A sandstone sample (MSE 136.5-137) was crushed and ground with an agate mortar and pestle, and then sieved to obtain the fraction between 50 and 100 μm. 10 grams of the resulting powder and 150 mL DI water were placed into a 200-mL polyethylene bottle and ultrasonic cleaned at least five times of 10-min per treatment. The bottle was immersed into a water bath to keep cool when ultrasonicating. The supernatant was disposed and the remaining solid was freeze dried. Selected sand stone particles were dispersed onto a double stick tape which is mounted on a glass slide. The sample was carbon coated before observation under SEM.

3.2. Batch Experiments

The prepared grains (feldspar, sandstone, etc.) were placed in a flexible gold reaction cell with detachable Ti-closure (Seyfried et al., 1987). This arrangement allows easy access to the reactants at the end of an experiment. More importantly, the flexible cell permits **on-line sampling of the aqueous phase at constant temperature and pressure** simply by adding water, in an amount equivalent to the sampled fluid, to the region surrounding the reaction cell (Fig. 2). These experimental data are generally superior to those derived from samples collected after the reactors are cooled down because backward reactions may occur during cooling.

The experiments using the flexible cell system were conducted at temperature of 200 °C and 300 bars. Fluid samples taken from the reactor at regular intervals were analyzed for all major and some minor dissolved components. Dissolved cations were analyzed by inductively coupled plasma mass spectrometry (ICP-MS), while anions were analyzed by ion chromatography.

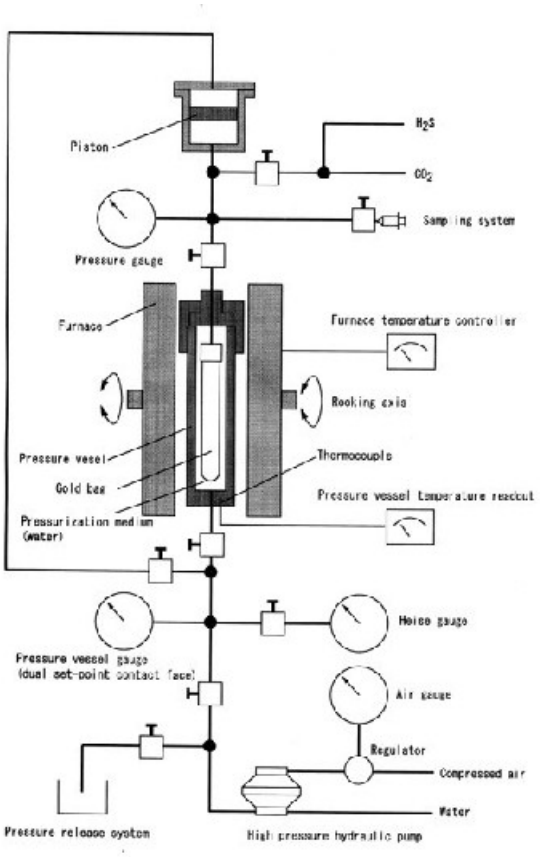

Figure 2. Schematic illustration of the flexible cell reaction system (Seyfried et al., 1987), which is being used for the mineral dissolution/precipitation rate studies.

The measured fluid chemistry including pH, when considered with distribution of aqueous speciation, taking explicit account of mass balance, mass action and charge balance constraints, together with constrains imposed by the revised HKF equation of state (Shock and Helgeson, 1988; Shock et al., 1989; Johnson et al., 1992; Shock et al., 1992; Sverjensky et al., 1997), permits calculation of ion activities of dissolved species.

3.3. Flow-through Experiments

The prepared sandstone grains were placed in a one-pass, tubular flow-through circulation apparatus. All wetted parts, with the exception of the back-pressure regulator (316 stainless steel), were constructed of high grade titanium in order to limit the effects of corrosion. Inflowing solutions were pumped by a HPLC pump at a rate of 0.82 ml/min. Solutions were preheated (to a maximum of 200°C) before contacting the sample, which resided midway in a tubular reactor. The horizontally-positioned reactor was heated independently by a tubular furnace. The system pressure was maintained at a constant value of 250 bars by the back-pressure regulator. The aqueous effluent was sampled at the downstream end of the regulator.

3.4. Electron Micro Beam Characterization of Reactants and Products

Reactants and products were investigated by an array of sophisticated techniques: gas adsorption (B.E.T surface area), SEM (phase relationships and surface morphology), electron microprobe, and XPS (surface chemistry), as well as High-resolution TEM (structure and chemistry).

Scanning Electron Microscopy (SEM) was conducted with a Philips XL 30 Field Emission Gun (FEG) SEM and an RJ Lee Instruments Personal SEM. The SEM has secondary and back scattered electron detectors for imaging, as well as an energy dispersive X-ray spectrometer with an EDAX ultrathin window CDU LEAP detector capable of analyzing light elements down to carbon. Feldspar grains were made into double-sided, polished petrographic thin-sections. The drill cutting samples were mixed with epoxy, secured into 1-inch phenol rings and gently polished to a smooth, flat surface. For grain mounts, sand grains were sprinkled onto double-sided tape. Samples were coated with a layer of carbon before SEM analysis. The compositions of feldspars were determined by wavelength dispersive X-ray spectroscopy using a CAMECA SX50 electron microprobe.

TEM observations were performed using a Philips CM300FEG microscope operated at 295 kV and a JEOL 2010 microscope operated at 200 kV. X-ray microanalyses were performed using a Philips EM 420 microscope equipped with an Oxford Si (Li) energy-dispersive X-ray system (EDS) and analytical software Desk Top Spectrum Analyzer (DTSA) from the National Institute of Standards and Technology. Data reduction was carried out using the standard Cliff-Lorimer method implemented in the DTSA.

Two TEM sample preparation methods were used, crushing and ion milling. In the first method, samples were ground in an agate mortar, suspended in ethanol, and then dropped on holey carbon film supported by a standard Cu TEM grid and air-dried. In the second method, specimens were prepared by cutting from petrographic thin sections and mounted onto single-hole Cu grids. Cu grids were mounted on the focus area, and the sample was further thinned to ~100 nm, using an ion beam. Finally, a very thin carbon film was coated onto the ion milled samples.

4. Results and Discussion

4.1. Alkali-feldspar dissolution experiments

Five-day experiments were performed to complement the experiments completed in the first year (Experiments #1 and #2 in Table 1). The experimental conditions were the same, alkali-feldspar dissolution experiments with and without the presence of CO_2 at 200 °C, 300 bars. 40 grams KCl solution and 2 (with 50 mmol/kg CO_2) or 1.5 grams (without CO_2) treated alkali-feldspar sample were used in the experiments. The presence of CO_2 buffered the initial solution to pH 4.0, whereas the fluid of system without CO_2 was acidified to pH 3.1 (at 25 °C and 1 bar) by addition of dilute HCl. Time series changes in the fluid chemistry of two alkali-feldspar-fluid systems are presented in Table 2 and Figure 3 (without CO_2) and Table 3 and Figure 4 (with CO_2), respectively. For comparison, the results of the first year alkali-feldspar dissolution experiments are also listed (Tables 2 and 3). The results of the 5-day experiments were in excellent accordance to the experiments in first year (Tables 2 and 3).

For the alkali-feldspar-fluid system without CO_2, as anticipated from constraints imposed by the relative abundance of fluid and mineral used for the experiment, dissolved K^+ and Cl^- concentrations remained relatively constant (Table 2 and Figure 3). Although Alkali feldspars dissolution releases K^+ into solution, the amount of this K^+ represents a small fraction of that initially available in the fluid (200 mmol/kg). Accordingly, dissolved K^+ can be considered buffered throughout the experiment. In contrast, the dissolved concentrations of Na^+, $Ca^{2+}$and SiO_2 increase gradually as alkali-feldspar feldspars dissolution reaction proceeded (Table 2 and Figure 3). During the whole experiment, pH values increased with reaction progress (Table 2).

Table 2. Time-dependent changes in the composition of major dissolved species in aqueous fluid coexisting with alkali-feldspar at 200°C and 300 bars. The overall analytical error is ±5%. In-situ pH is calculated from distribution of aqueous species calculations at the temperature and pressure of the experiment using constraints imposed by major element concentrations and pH values measured at 25°C.

Time (days)	Cl^-	K^+	SiO_2	Na^+	Ca^{2+}	Al^{3+}	pH (25°C)	In-situ pH (200°C)
			(mmol/kg)					
0	198.3	204.0	-	-	3.72	-	3.0	3.1
1	197.5	202.8	0.31	0.42	0.12	0.01	3.2	3.3
5*			1.31	0.88	0.35	0.005	3.0**	
9	198.7	201.1	1.46	1.13	0.21	-	3.5	3.6
19	196.8	197.8	1.70	2.04	0.43	0.08	4.1	3.6
34	197.9	204.3	1.35	1.86	0.16	0.03	4.2	3.9
57	199.5	197.0	4.18	3.72	0.30	0.01	4.9	4.8
78	199.4	196.5	3.75	1.91	0.35	-	4.9	4.9

Note: Except the data of the 5-day experiments, all the data were from experiments performed in year one. The data are slightly different from those in the first year's report because we re-measured some samples and got new data. *5-day alkali-feldspar dissolution experiment without CO_2 at 200 °C and 300 bars. ** Starting pH measured at room temperature.

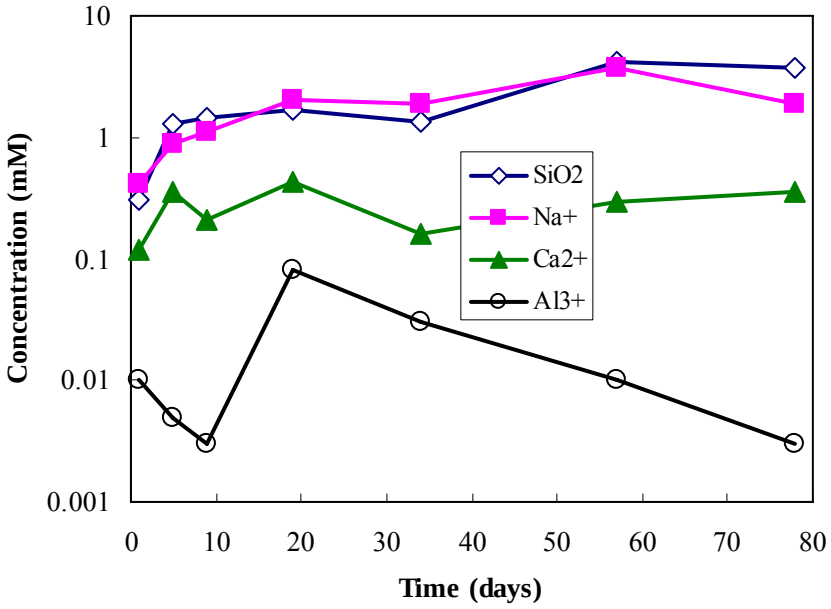

Figure 3. Experimental results of change in Na, Si, Ca and Al concentrations with time during the course of alkali-feldspar dissolution without the presence of CO_2.

For the alkali-feldspar-fluid system with CO_2, the dissolved concentrations of Na^+, $NH_4^+$and SiO_2 increase gradually as the alkali-feldspar dissolution reaction proceeded and dissolved K^+ and Cl^- concentrations remained relatively constant (Table 3 and Figure 4).

Table 3. Time-dependent changes in the composition of major dissolved species in aqueous fluid coexisting with Alkali-feldspar at 200°C and 300 bars in the presence of CO_2. The overall analytical error is ±5%.

Time (days)	Cl^-	K^+	SiO_2	Na^+	Ca^{2+}	Al^{3+}	pH (25°C)
			(mmol/kg)				
1	199.2	196.3	0.40	0.26			4.3
5*		159.1	1.96	1.89	0.16	0.006	4.0**
6	196.5	194.3	1.88	0.45			4.5
13	197.5	195.4	2.30	0.93			5.0
20	199.4	196.2	2.42	1.41			5.1
27	198.8	195.4	2.49	0.97			5.1

Note: Except the data of 5-day experiments, all the data were from experiments performed in year one.
*5-day alkali-feldspar dissolution experiment with CO_2 at 200°C and 300 bars. ** Starting pH at room temperature.

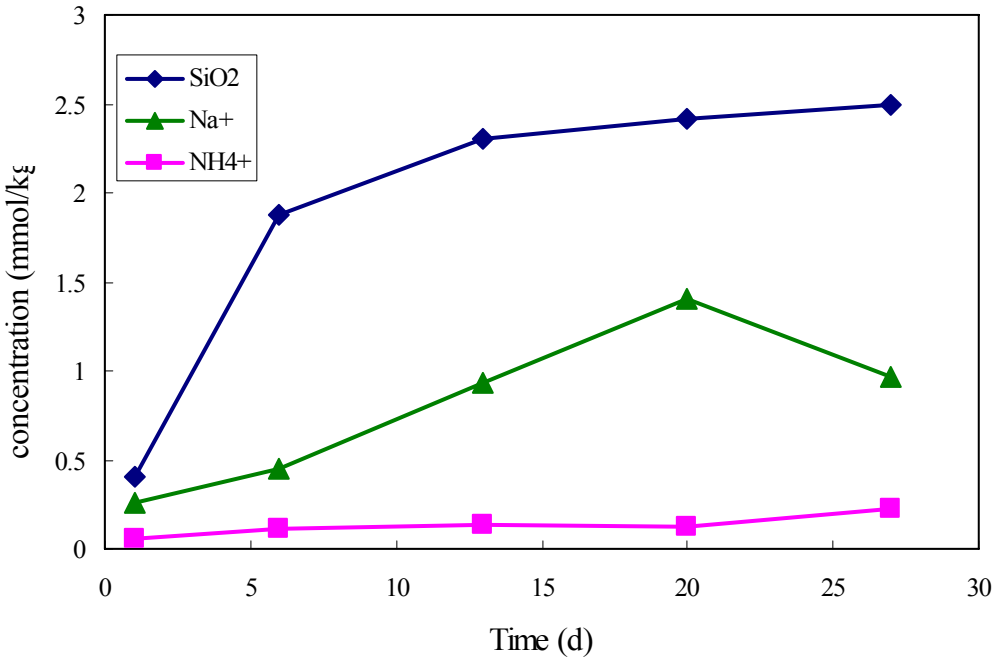

Figure 4. Experimental results of change in Na, Si, and NH_4^+ concentrations with time during the course of alkali-feldspar dissolution with the presence of CO_2.

SEM photomicrographs (see figure 5) of products following batch dissolution experiments show dissolution etch pits, demonstrating that dissolution has occurred. Larger and deeper etch pits and more secondary minerals are observed on the feldspar grains after Experiment 1 (with CO_2) than after Experiment 2 (without CO_2), showing that Experiment 1 reacts more extensive than Experiment 2.

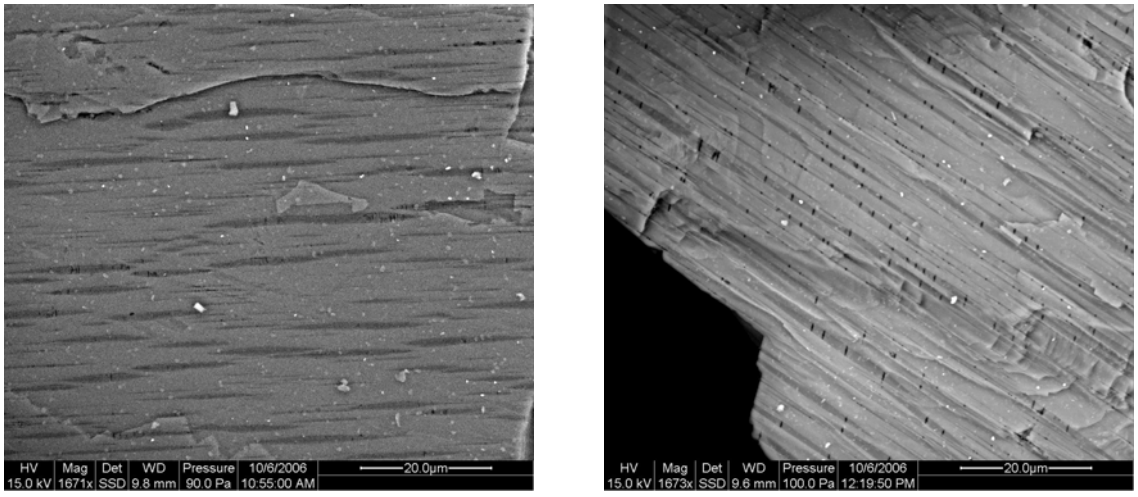

Figure 5. SEM backscatter electron micrographs show that the same feldspar particles after the hydrothermal reaction experiment. left: without CO_2; right: with CO_2.

The surface chemistry of alkali-feldspar was analyzed as well by X-ray photoelectron spectroscopy (XPS), before and after the experiment for the alkali-feldspar-fluid system without CO_2 (exp 2). Results showed that the K/Al and Al/Si mole ratios are 0.66 and 0.37, respectively before the experiment (Table 4), which is consistent with electron microprobe analysis results. The Al/Si mole ratio increased significantly to 1.06 after the experiment, while K/Al decreased to 0.35. The increase of Al/Si and the decrease of K/Al on the alkali-feldspar surface following the experiment indicate the existence of a secondary mineral phase in which Al has higher compositional percentage than in "K-feldspar" or albite at the alkali-feldspar-fluid interface.

Table 4. XPS surface composition results* of alkali-feldspar from experiment in comparison with theoretical values for "K-feldspar" and kaolinite. The data indicate a significant increase in Al/Si consistent with the existence of aluminum rich secondary phase at the alkali-feldspar-fluid interface.

	K	Al	O	Si	K/Al	Al/Si
	mole%				mole ratio	mole ratio
Starting alkali-feldspar	5.7	8.7	62.2	23.4	0.66	0.37
Alkali-feldspar Product	5.7	16.3	62.6	15.4	0.35	1.06
K-feldspar	7.7	7.7	61.5	23.1	1	0.33
Kaolinite	-	20.9	55.8	21.8	-	1

*Each result reflects the average value of 4 measurements from different alkali-feldspar grains within the same sample.

4.2. "K-feldspar" dissolution experiments

A batch experiment involving "K-feldspar" dissolution in Na-bearing (~0.05 NaCl mol/kg) fluid at 200 °C, 300 bars with the presence of CO_2 (6.0 mmol/kg) was conducted at the University of Minnesota. Time series changes in the fluid chemistry of K-feldspar-fluid systems are shown in Table 5 and Figure 6. The dissolved concentrations of K^+ and SiO_2 increase gradually as K-feldspars dissolution reaction proceeded and dissolved Na^+ and Cl^- concentrations remained relatively constant (Table 5 and Figure 6). Except at 28 day, the Al^{3+} concentration remained low during the course of feldspar dissolution (Table 5 and Figure 6). During the whole experiment, pH values increased with reaction progress (Table 5). X-ray diffraction and microprobe results show that K-feldspar sample was composed of 30% low albite and 70% microcline. Multipoint N_2 gas adsorption isotherms were measured to obtain the specific surface area of 0.129 m^2/g for feldspar.

Table 5. Time-dependent changes in the composition of major dissolved species in aqueous fluid coexisting with "K-feldspar" at 200 °C and 300 bars. The overall analytical error for dissolved species is ±5%. In-situ pH is calculated from distribution of aqueous species calculations at the temperature and pressure of the experiment using constraints imposed by major element concentrations and pH values measured at 25°C.

Sample	Time (days)	Na^+	Mg^{2+}	K^+	SiO_2	Al^{3+}	Ca^{2+}	Li^+	NH_4^+	Cl^-	CO_2(aq)	pH 25°C	pH In-situ*
		(mmol/kg)											
starting	0	50.22	0.01	0	0	0	0.03	0	0.01	48.18		-	-
#1	1	50.03	0.01	0.37	1.40	0.02	0.03	0.01	0.05	48.41	6.1	5.3	6.1
#2	17	49.87	0.01	0.87	2.80	0.03	0.03	0.01	0.05	49.53	6.2	5.4	6.2
#3	28	49.50	0.05	0.87	2.92	0.18	0.13	0.01	0.04	49.97	6.0	5.5	6.2
#4	49	49.63	0.01	0.80	2.86	0.02	0.17	0.01	0.05	49.85	6.2	5.6	6.4
#5	77	50.13	0.02	0.79	2.72	0.03	0.05	0.01	0.18	49.80	6.1	5.4	6.2
#6	141	50.65	0.02	1.01	3.04	0.02	0.05	0.01	0.14	50.11	6.1	5.7	6.6

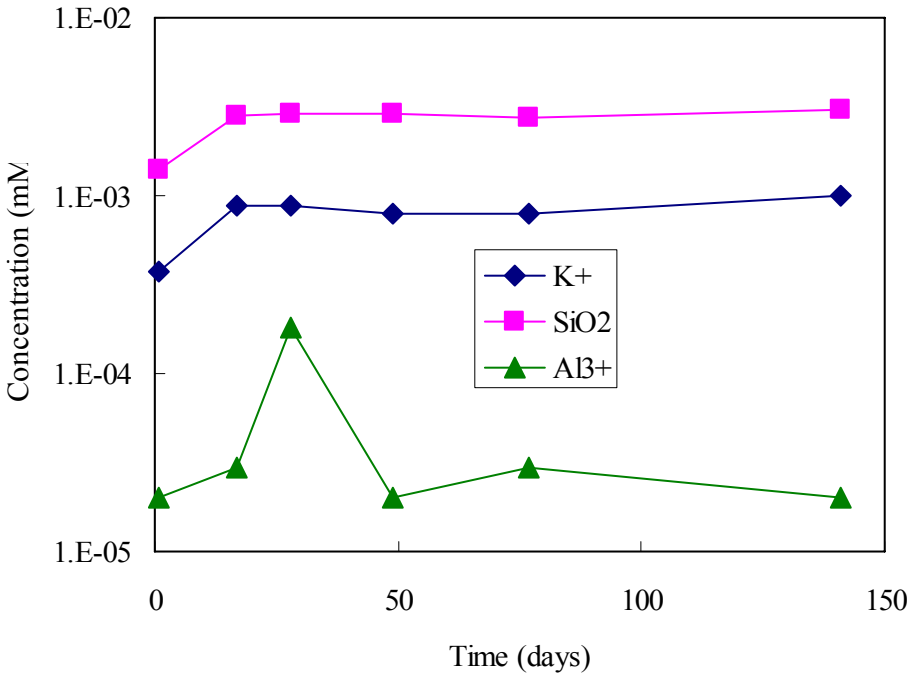

Figure 6. Experimental results of change in K, Si, and Al concentrations with time during the course of "K-feldspar" dissolution with the presence of CO_2.

XPS analysis was performed on starting "K-feldspar" mineral and experiment products. Results showed that the Al/Si mole ratios changed significantly from 0.37 to 0.75 in experiment with CO_2-bearing aqueous fluid at relatively high pH, and to 1.06 without dissolved CO_2 at relatively low pH, respectively (Table 6). The increase of Al/Si of "K-feldspar" surface following the experiment was consistent with the existence of aluminum rich secondary phase at the K-feldspar-fluid interface.

Table 6. XPS surface composition results* of "K-feldspar" from experiments in comparison with theoretical values for "K-feldspar" and muscovite.

	K	Al	O	Si	Al/Si
		mole%			mole ratio
Starting K-feldspar	5.7	8.7	62.2	23.4	0.37
"K-feldspar" Product#1†	5.3	13.6	62.9	18.2	0.75
"K-feldspar" Product#2§	5.7	16.3	62.6	15.4	1.06
K-feldspar	7.7	7.7	61.5	23.1	0.33
Muscovite	5.3	15.8	63.1	15.8	1

*Each result reflects the average value of 4 measurements from different "K-feldspar" grains within the same sample.

† Dissolution of "K-feldspar" with CO_2-bearing aqueous fluid at relatively high pH at 200°C and 300 Bars.

§ Dissolution of "K-feldspar" without dissolved CO_2 at relatively low pH at 200°C and 300 Bars.

4.3. Navajo Sandstone Experiments

Our second set of experiments was on Navajo Sandstone, to test the feasibility of using red beds as storage of mixed CO_2. We have completed the three experiments and measured the major and trace element concentrations of the fluids from the hydrothermal experiments.

The first Navajo Sandstone dissolution experiment was a batch experiment at 200°C and 300 Bars. The major mineral component of Navajo Sandstone is quartz, with ~2% feldspars (Harshbarger et al., 1957; Dulaney, 1989; Zhu, 2005). 4 grams of Navajo sandstone were reacted with 40 grams 200 mmol/kg KCl solution in the presence of 20 mmol/kg CO_2 (aq). The results are presented in Table 7 and 8. During the experiment, dissolved K^+ and Cl^- concentrations remained relatively constant (Table 7). Dissolved SiO_2 increased, reaching 2.20 mmol/kg by the end of experiment. The dissolved concentrations of Mg^{2+} also increased with time. There was almost no change for dissolved CO_2 concentration throughout the experiment, while pH values increased slowly with reaction progress. Generally, the dissolved concentrations of most of minor and trace elements approached steady-state values within first 48 hours (Table 8).

Table 7. Time-dependent changes in the composition of major dissolved species in CO_2-bearing aqueous fluid coexisting with Navajo sandstone at 200 °C and 300 bars. The overall analytical error for dissolved species is ±5%. In-situ pH is calculated from distribution of aqueous species calculations at the temperature and pressure of the experiment using constraints imposed by major element concentrations and pH values measured at 25°C.

Sample	Time	K^+	SiO_2	Al^{3+}	Na^+	Mg^{2+}	Ca^{2+}	NH_4^+	Cl^-	SO_4^{2-}	CO_2(aq)	pH	
	(days)					(mmol/kg)						25°C	In-situ*
starting	0	197.26	-	-	0.17	-	-	0.10	200.77	0.04	20.3	-	-
#1	2	195.00	0.89	0.01	0.26	0.09	0.29	0.25	193.33	0.16	19.2	4.7	5.5
#2	6	190.42	1.70	0.01	0.08	0.11	0.26	0.20	197.76	0.05	19.7	4.8	5.5
#3	14	193.32	2.03	0.10	0.14	0.17	0.34	0.27	192.38	-	19.5	4.9	5.5
#4	23	199.60	2.20	0.02	0.05	0.19	0.33	0.16	193.66	0.18	19.6	4.9	5.6

Table 8. Time-dependent changes in the composition of minor and trace dissolved species in CO_2-bearing aqueous fluid coexisting with Navajo sandstone at 200°C and 300 bars. The overall analytical error for concentration measurements is ±5%.

Sample	Li	Cr	Fe	Mn	Co	Ni	Cu	Zn	Rb	Sr	Cs	Ba
						(ppm)						
Starting	-	-	-	-	-	-	0.10	0.24	0.29	0.01	0.01	0.01
#1	-	-	1.70	0.09	0.01	-	0.06	0.32	0.27	0.36	0.01	0.22
#2	-	-	-	0.08	-	-	0.13	0.20	0.27	0.36	0.01	0.30
#3	0.04	0.01	6.63	0.13	0.01	0.25	0.27	0.38	0.43	0.36	0.08	0.25
#4	0.05	-	0.67	0.12	-	0.18	0.09	0.17	0.32	0.35	0.02	0.24

The second Navajo Sandstone dissolution experiment was a batch experiment at 200°C and 300 Bars. 4 grams of Navajo sandstone were reacted with 40 grams 200 mmol/kg KCl solution without the presence CO_2 (aq) at pH 3. The results are presented in Tables 9 and 10. During the experiment, dissolved K^+ and Cl^- concentrations remained relatively constant (Table 9). Dissolved SiO_2 increased, reaching 4.0 mmol/kg at 7 day, suggesting that sandstone dissolved much faster in the system without CO_2 compared with the sandstone-CO_2 system. The dissolved concentrations of Mg^{2+} also increased with time. pH values increased fast with reaction progress. Generally, the dissolved concentrations of most of minor and trace elements approached steady-state values within first 24 hours (Table 10).

Table 9. Time-dependent changes in the composition of major dissolved species in aqueous fluid coexisting with Navajo sandstone at 200°C and 300 bars. The overall analytical error for dissolved species is ±5%. In-situ pH is calculated from distribution of aqueous species calculations at the temperature and pressure of the experiment using constraints imposed by major element concentrations and pH values measured at 25°C (see text).

Sample	Time	K^+	SiO_2	Al^{3+}	Na^+	Mg^{2+}	Ca^{2+}	NH_4^+	Cl^-	pH	
	(days)				(mmol/kg)					25°C	In-situ*
starting	0	203.86	-	-	0.11	-	-	0.11	188.25		
#1	1	197.28	1.63	0.14	1.42	0.77	1.15	0.07	184.91	3.6	3.3
#2	7	200.07	4.00	0.03	0.14	1.03	1.17	0.07	182.93	4.6	4.0

Table 10. Time-dependent changes in the composition of minor and trace dissolved species in aqueous fluid coexisting with Navajo sandstone at 200°C and 300 bars. The overall analytical error for concentration measurements is ±5%.

Sample	Li	Cr	Fe	Mn	Co	Ni	Cu	Zn	Rb	Sr	Cs	Ba
						(ppm)						
Starting	-	-	-	-	-	-	-	0.04	0.12	0.01	0.01	0.04
#1	-	-	1.57	0.94	-	-	6.07	0.52	0.12	0.54	0.01	0.41
#2	-	-	0.10	0.75	-	0.09	0.10	0.20	0.13	0.54	0.01	0.30

The third Navajo Sandstone dissolution experiment was a flow-through experiment at 200°C and 250 Bars. 5 grams of Navajo sandstone were reacted with 200 mmol/kg KCl solution without the presence CO_2 (aq) at pH 3.9. The flow rate is 0.82 ml/min. The results are presented in Table 11. During the experiment, dissolved K^+ and Cl^- concentrations remained relatively

constant (Table 11). The dissolved concentrations of Si and Mg approached steady-state values within first 4 hours. pH values increased slowly with reaction progress.

Table 11. Time-dependent changes in the composition of major dissolved species in aqueous fluid coexisting with Navajo sandstone at 200°C and 300 bars. The overall analytical error for dissolved species is ±5%. In-situ pH is calculated from distribution of aqueous species calculations at the temperature and pressure of the experiment using constraints imposed by major element concentrations and pH values measured at 25°C.

Sample	Time	K^+	SiO_2	Al^{3+}	Na^+	Mg^{2+}	Ca^{2+}	Cl^-	pH	
	(hours)				(mmol/kg)				25°C	In-situ*
#1	0.5	196.35	0.02	-	0.22	0.01	0.02	201.43	5.2	5.0
#2	4	209.45	0.26	-	0.02	0.04	-	198.79	5.3	5.1
#3	13	207.01	0.24	-	0.05	0.03	0.01	197.34	5.3	5.1
#4	23.5	204.83	0.18	-	0.30	0.05	0.02	196.78	5.5	5.2

Dissolution rate was calculated according to the following formula based on time-series Si concentrations:

$$r = \frac{(C_{out})(\vartheta_0)(10^{-6})}{M\delta A}$$

where C_{out} is the output concentration of Si in mg/L, ϑ_0 is the input flow rate in ml/s, M is the atomic weight (g/mol) of Si, δ is the stoichiometric coefficient of Si in quartz, and A is the total surface area in m^2/g. The average dissolution rate is 6.85×10^{-10} mol $m^{-2}s^{-1}$ (Table 12).

Table 12. Dissolution rates of Navajo sandstone in the experiment with flow-through apparatus at 200°C and 250 bars. The total surface area of 5 gram Navajo sandstone is assumed to be 3.5 m^2. The input flow rate is 0.82 ml/min.

Sample	Dissolution Rate (mol $m^{-2}s^{-1}$)
#1	7.79×10^{-11}
#2	1.03×10^{-9}
#3	9.33×10^{-10}
#4	7.01×10^{-10}
Average	6.85×10^{-10}

SEM photomicrographs of products following batch dissolution experiments (Figures 8 and 10) were compared with reactants (Figure 7). EDS results confirmed that these particles shown in Figure 8 are quartz (Figure 9). Some secondary minerals were formed between sandstone particles, demonstrating that dissolution has occurred (Figures 8 and 10). According to the EDS results, the secondary minerals could be clay and Fe-bearing minerals (siderite, $FeCO_3$).

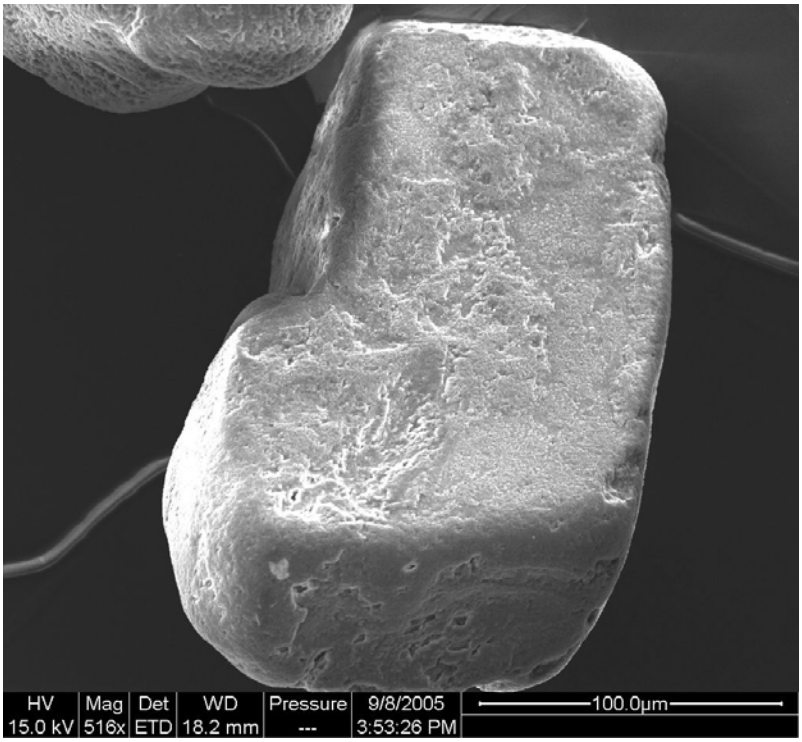

Figure 7. SEM micrograph shows that Navajo sandstone before the hydrothermal experiment.

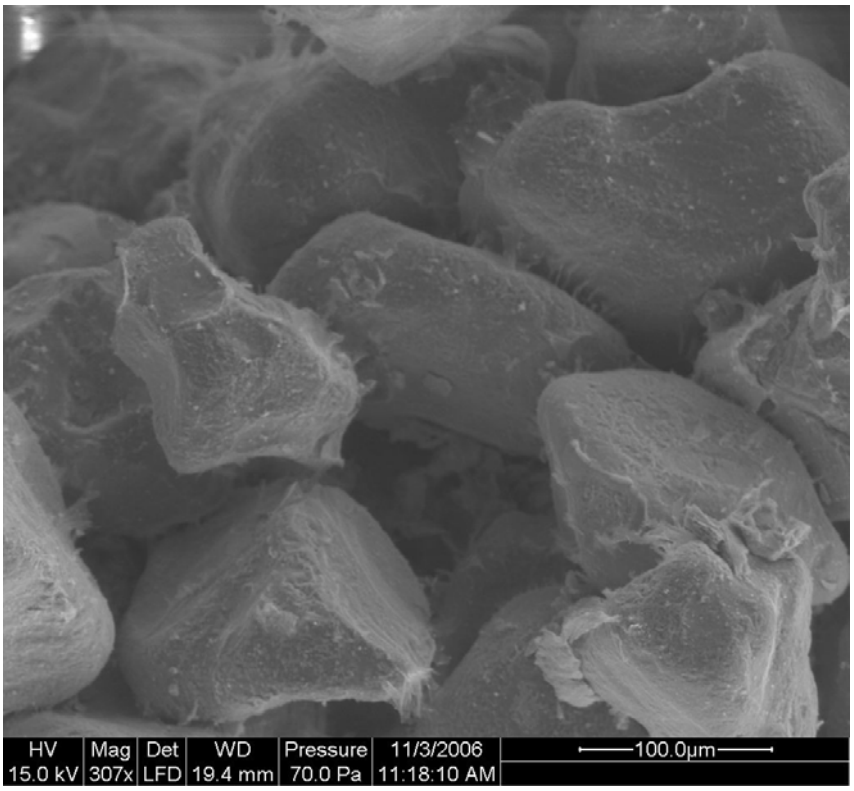

Figure 8. SEM micrograph shows that Navajo sandstone after the hydrothermal experiment.

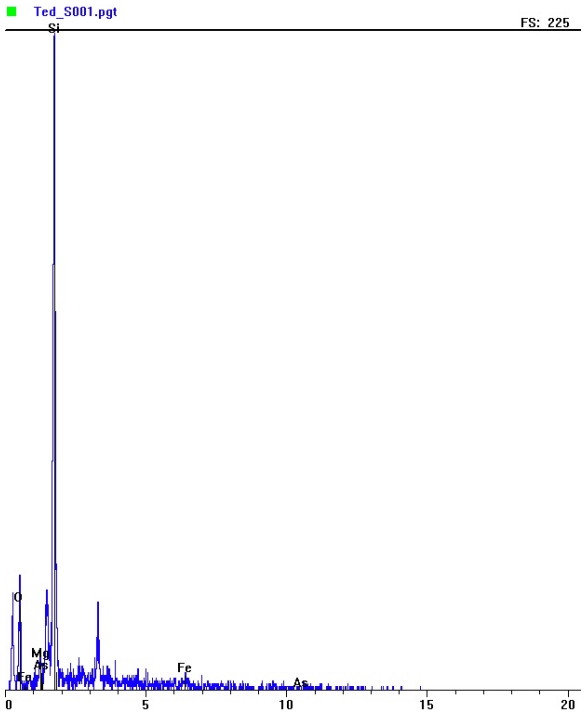

Figure 9. EDS results confirmed that these particles shown in Figure 8 are quartz.

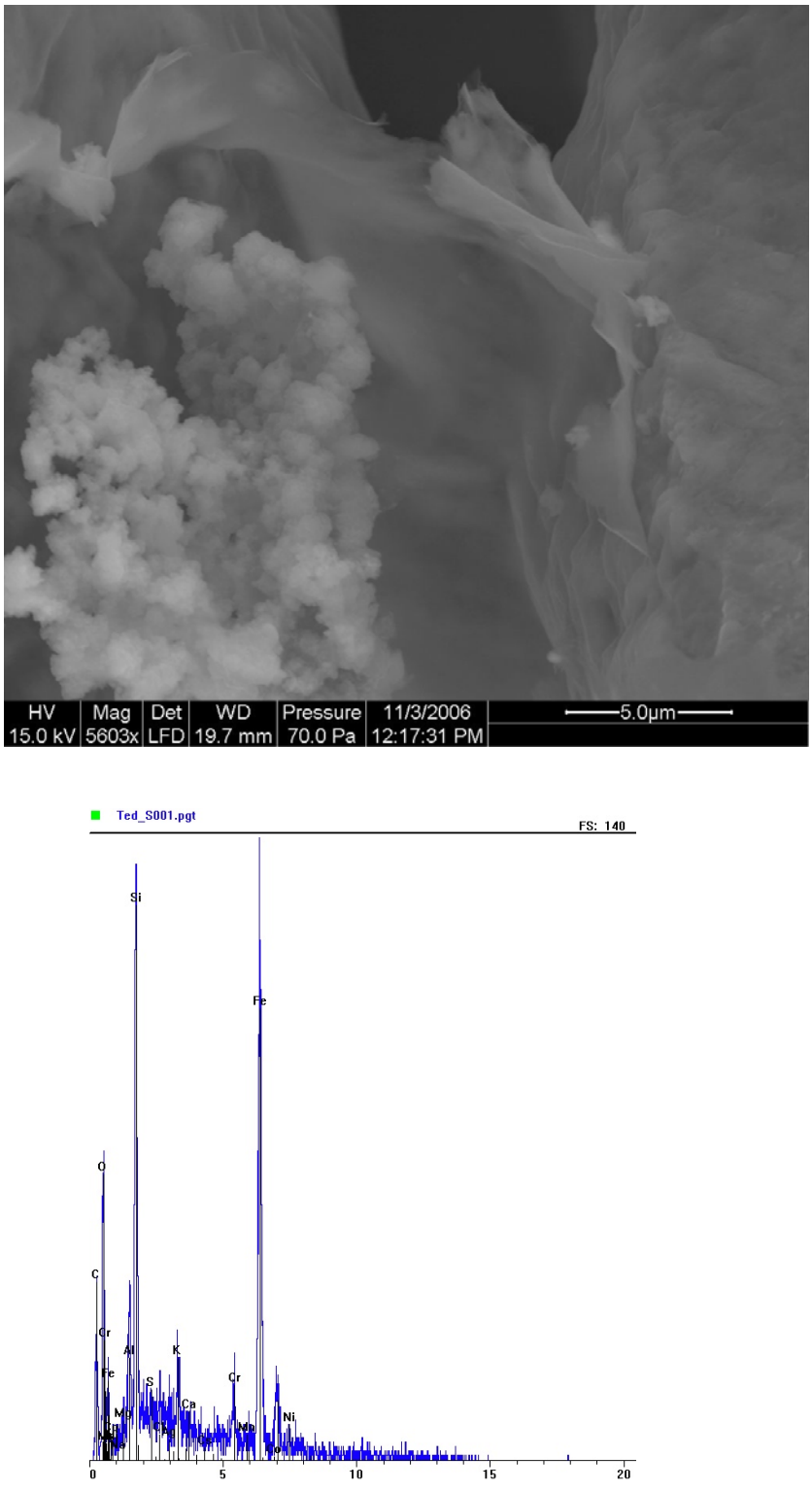

Figure 10. SEM micrograph (upper) shows the connection part of two quartz particles after the hydrothermal experiment. Fe particles and the "film" are visible. EDS (lower) shows the chemical compositions of Fe particles (siderite, $FeCO_3$).

4.5. Geochemical Modeling

We accomplished the modeling of alkali-feldspar-fluid system without CO_2, and established a procedure for geochemical modeling of hydrothermal experiments, which includes building up a thermodynamic database at temperature and pressure of interest, calculating reaction constants of aqueous specious dissociation and mineral formation reactions, constructing a phase diagram, calculating saturation indices, and performing reaction path-modeling. In addition, numerical modeling of "K-feldspar" dissolution and alkali-feldspar-fluid system with CO_2 are on-going. The following materials focus on reaction path models of alkali-feldspar-fluid system without CO_2. As stated before Ab and Ksp refer to Na-rich ($Ca_{0.04}Na_{0.95}K_{0.01}Al_{1.04}Si_{2.96}O_8$) and K-rich ($K_{0.85}Na_{0.15}Al_{1.04}Si_{2.97}O_8$) lamellae of alkali-feldspar.

Reaction path models calculate a sequence of equilibrium states or steady states involving incremental or step-wise mass transfer between the phases within a system, or incremental addition or subtraction of a reactant from the system (Helgeson, 1968b; Helgeson et al., 1969a). The calculated mass transfer is based on the principles of mass balance, partial and local equilibrium, and reaction kinetics.

Feldspar hydrolysis is the system in which (Helgeson, 1968b) developed the reaction-path modeling approach. Although the original example was based on local and partial equilibrium (Helgeson, 1968b; Helgeson et al., 1969a; Helgeson, 1979). HELGESON and MURPHY (1983) added feldspar dissolution kinetics into the model. LASAGA (1998) further showed that different reaction paths will result from different relative rates of feldspar dissolution and secondary mineral precipitation.

Reaction path calculations were carried out to examine feldspar dissolution and secondary minerals precipitation processes. In the K_2O-Al_2O_3-SiO_2-H_2O-HCl activity-activity diagram, reaction path starts from boehmite field, through kaolinite field, to muscovite field, and approaching microcline field. In the Na_2O-Al_2O_3-SiO_2-H_2O-HCl activity-activity diagram, the reaction path starts from boehmite field, but terminates in kaolinite field. Boehmite, kaolinite, and muscovite are considered as the secondary minerals. The simulation of Ab dissolution rates with rate equation adapted from Burch et al. (1993) is consistent with average rates of alkali-feldspar based on the change of Si concentration from experimental data. The saturation indices of both the simulations of Ab and Ksp dissolution process are consistent with those calculated based on experimental data. Following Hellmann and Tisserand (2006), the R-ΔG_r rates curve was divide into 3 distinct regions: the "far-from-equilibrium" region ($\Delta G_r < -69$ KJ mol^{-1}), the "transition equilibrium" region ($-69 \leq \Delta G_r \leq -25$ kJ mol^{-1}), and the "near equilibrium" region ($\Delta G_r > -25$ kJ mol^{-1}). The curve of [Si]:[Al] stoichiometry with ΔG_r is inconsistent with data from the experiment and saturation indices of secondary minerals (boehmite, kaolinite, and muscovite) do not match well with the saturation indices calculated with solution chemistry data, especially during the early stage of precipitation, implying that the simple rate law (based on transition state theory) we used was incapable to simulate the real situation of secondary minerals precipitation. The amounts of boehmite, muscovite, and kaolinite increase gradually from 0 to 2.42×10^{-4}, 3.2×10^{-4}, and 1.69×10^{-4} moles respectively during the course of 78 days' simulation.

The calculated and analyzed concentrations of Al, Si, and Na as a function of time are compared in Fig. 11a. After a short period (4 days) of a very steep increase in Si and Na concentrations, a less steep and almost constant increase of concentrations is observed, which is

consistent with experimental data. The calculated Al concentrations before 19 days are inconsistent with measured Al data. A gradual decrease in calculated Al concentrations after a steep increase in the first 3.5 days was observed. But an increase in Al concentrations during 9 to 19 days was found in the experimental data (Fig. 11a). The inconsistence may be due to the uncertainty of Al analysis and the simple rate law (based on transition state theory) we used for secondary mineral precipitate was incapable to predict the secondary minerals precipitation rates in the first 19 days' reaction.

The calculated pH (Fig. 11b) is gradually increased from 3.1 to about 5.1 with the reaction progress, which is consistent with experimental results.

The changes with time in Ab dissolution rates are shown in Fig 12a. During the first day simulation, the solution is highly undersaturated with respect to Ab. After this stage, the rate decreased sharply for about half order of magnitude during 1 to 4 days, corresponding to rapid change in saturation indices from -6.4 to -4.3 (Fig. 17). Ab dissolution rates decrease slowly for about 1 order of magnitude until the end of the simulation (SI change from -4.3 to -1.6). In contrast, Ksp dissolution rates (Fig. 12b) drop sharply for about 2 orders of magnitude at the first 3 days corresponding to saturation indices changing rapidly from -6.3 to -0.92. After that the rates decrease slowly for about 2 orders magnitude during 3 to 15.5 days, corresponding to saturation indices change from -0.92 to 0 (equilibrium). After the solution is saturated with respect to Ksp, Ksp rates decrease sharply until the rate plateau (from 16 to 78 day) is reached. Thermodynamically, Ksp dissolution is suppressed because dissolution of Ksp will compete with dissolution of Ab. Only dissolution of one mineral is allowed and Ab dissolution is thermodynamically favored. However, kinetically, both Ab and Ksp tend to dissolve, and are controlled by different dissolution rates. A total of 9×10^{-6} moles of Ksp and 1.179×10^{-3} moles of Ab dissolve during entire simulation. Ab dissolution is the dominant process and its rates are comparable with average rates of alkali-feldspar based on the change of Si and Na concentration from experimental data (Fig. 12a).

Fig. 13 shows calculated rates of Ab dissolution vs. ΔG_r. The R-ΔG_r rates curve is highly non-linear and show a sigmoidal trend and are characterized by three distinct regions (Hellmann and Tisserand, 2006), whose exact limits are somewhat subjective: $\Delta G_r < -70$ KJ mol^{-1} represents "far-from-equilibrium" dissolution and a rate plateau, here the rates are constant (7.1×10^{-10} mole $m^{-2}s^{-1}$) and independent of ΔG_r; the "transition equilibrium" region, $-70 \leq \Delta G_r \leq -25$ kJ mol^{-1}, characterized by a sharp decrease in dissolution rates (from 7.1×10^{-10} to 7.4×10^{-11} moles $m^{-2}s^{-1}$) with increasing ΔG_r, indicating a strong inverse dependence on ΔG_r; the "near equilibrium" region, $\Delta G_r > -25$ kJ mol^{-1}, where the rates (decreased from 7.4×10^{-11} to 2.0×10^{-11} mole $m^{-2}s^{-1}$) show a much less pronounced inverse dependence on ΔG_r. Note that the hypothetical datum R = 0, $\Delta Gr = 0$ represents chemical equilibrium. It took about 19.8 year to approach chemical equilibrium in our simulation. Hellmann and Tisserand (2006) showed the same type of curve. The calculated Ab dissolution rates are comparable to average rates of alkali-feldspar based on experimental data of Si as a function of ΔG_r. (As ΔG_r is a function of time, the sampling times are converted to ΔG_r values from simulation).

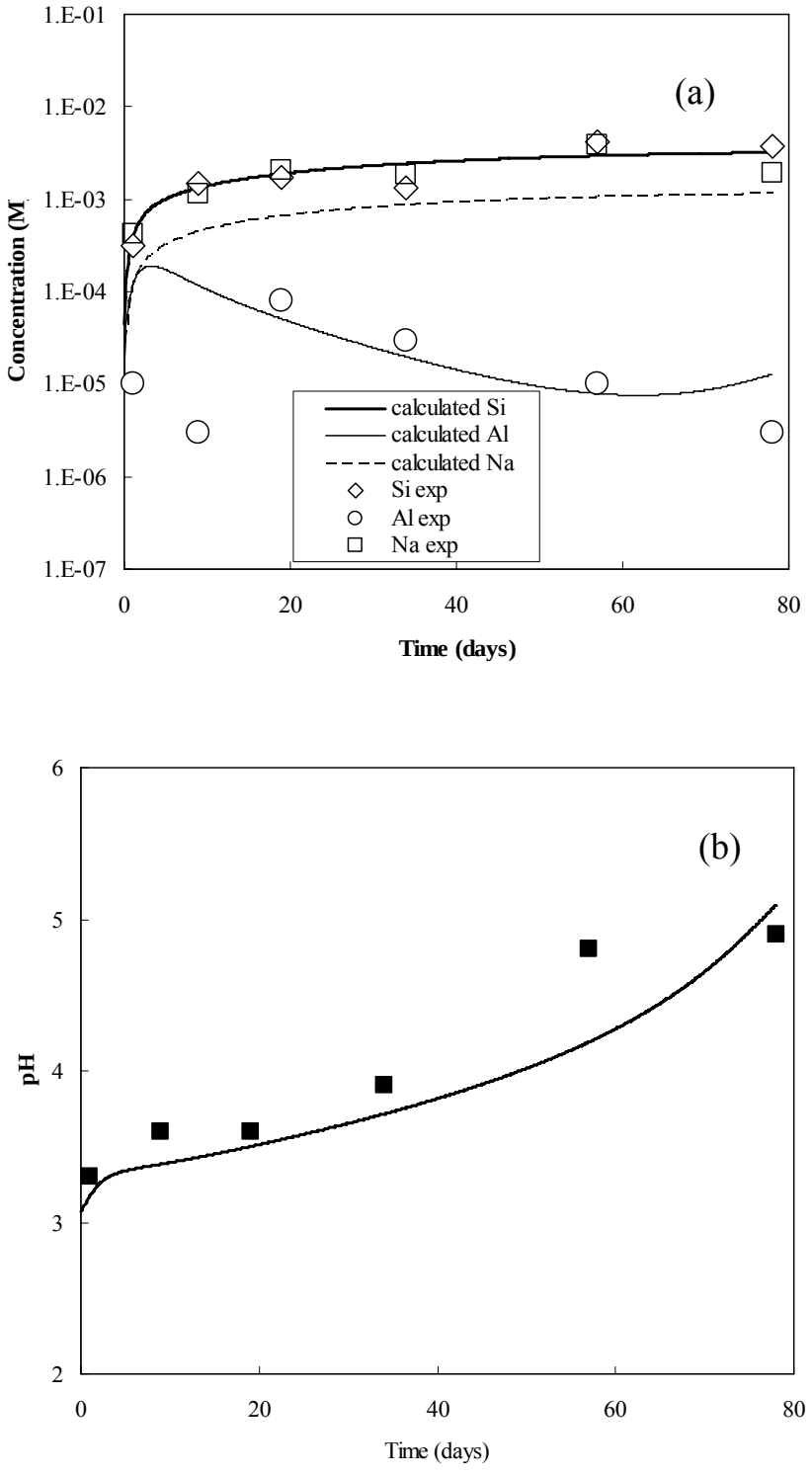

Figure 11. The calculated change in Na, Si and Al concentrations (a) and pH evolution (b) compared with experimental data with time during the course of alkali feldspar dissolution. Secondary phases are allowed to precipitate in this simulation.

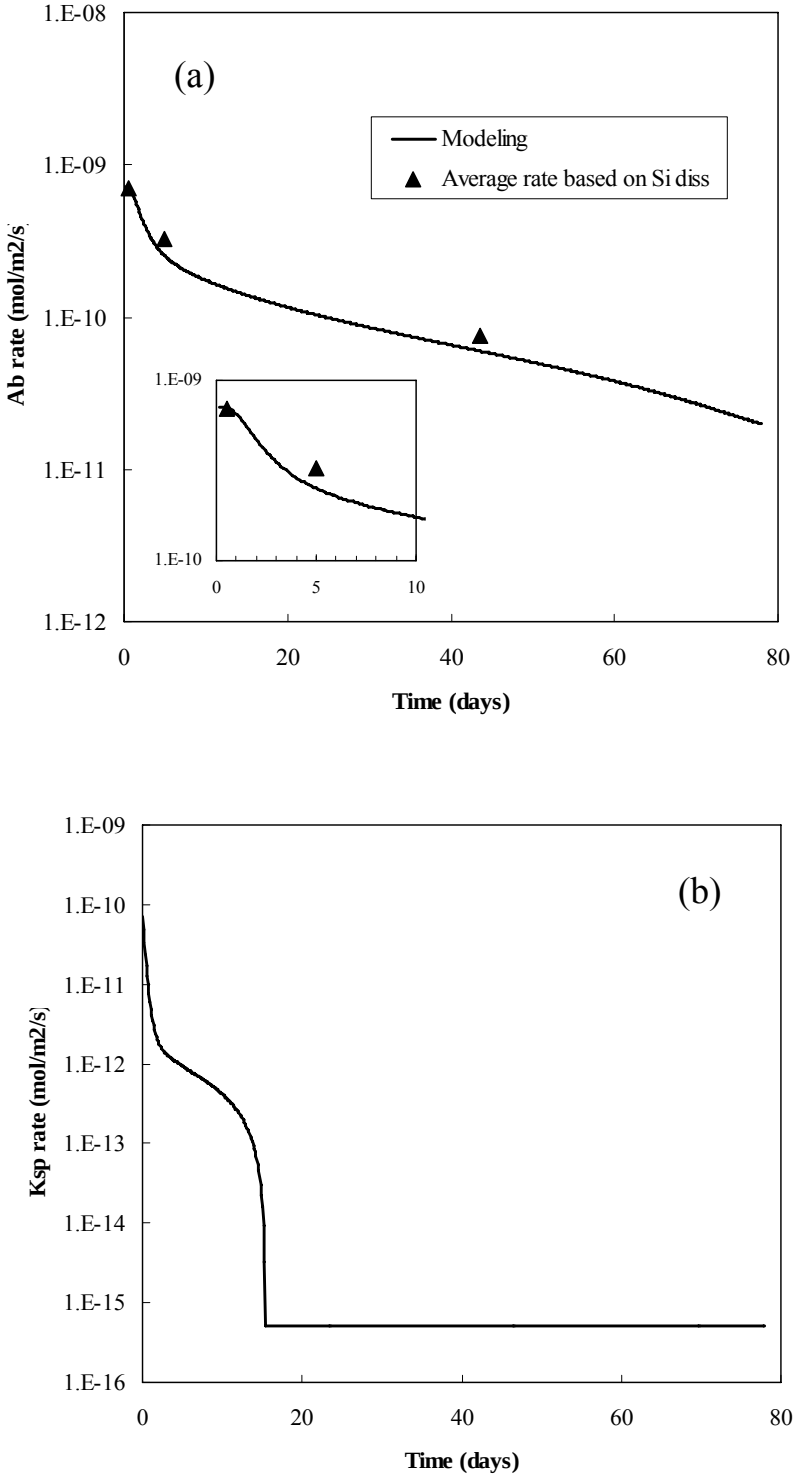

Figure 12. The calculated change in (a) Ab and (b) Ksp dissolution rates with time during the course of alkali feldspar dissolution. Secondary phases are allowed to precipitate in this simulation. Ab dissolution rates are comparable to average rates of alkali-feldspar based on experimental data of Si and Na.

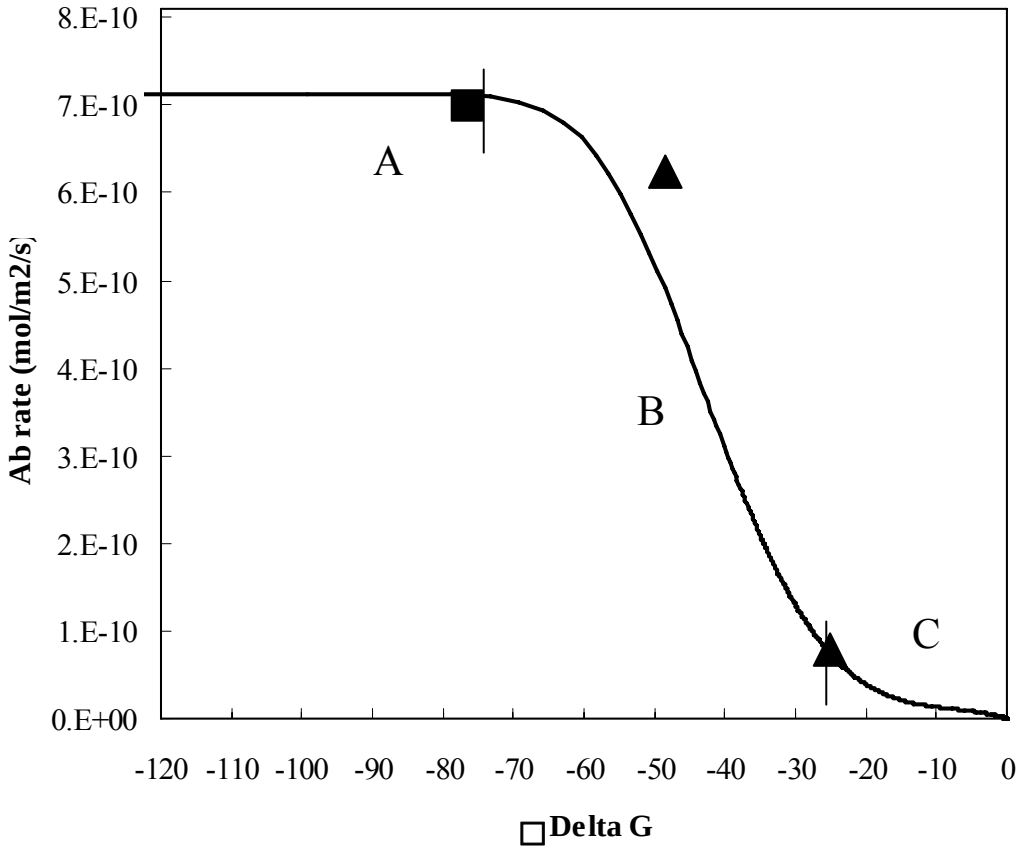

Figure 13. Calculated rates of Ab dissolution based on an overall rate expression (Eq.(5)) composed of two parallel rate laws as a function of ΔG_r, compared to average rates of alkali-feldspar based on experimental data of Si and Na (as ΔG_r is a function of time, the sampling times are converted to ΔG_r values from simulation). The R-ΔG_r rates curve are highly non-linear and show a sigmoidal trend, and are characterized by three distinct regions, whose exact limits are somewhat subjective: $\Delta G_r < -75$ KJ mol^{-1} represents "far-from-equilibrium" dissolution and a rate plateau, here the rates are constant and independent of ΔG_r, Al]; the "transition equilibrium" region, $-75 \leq \Delta G_r \leq -25$ kJ mol^{-1}, characterized by rates with a strong inverse dependence on ΔG_r; the "near equilibrium" region, $\Delta G_r > -25$ kJ mol^{-1}, where the rates show a much less pronounced inverse dependence on ΔG_r. Note that the hypothetical datum R = 0, ΔGr = 0 represents chemical equilibrium.

Fig. 14 shows Si:Al ratio as a function of ΔG_r compared with experimental data (as ΔG_r is a function of time, the sampling times are converted to ΔG_r values from simulation). At the "far-from-equilibrium" conditions, $\Delta G_r < -70$ kJ mol^{-1}, the [Si]:[Al] value of the experiment is much higher than the calculated one, implying the incongruent dissolution behavior. At "transition equilibrium" region ($-70 \leq \Delta G_r \leq -25$ kJ mol^{-1}), the calculated [Si]:[Al] ratio increased sharply after a relatively stable [Si]:[Al] values at the early stage, implying that the large amount of secondary minerals precipitate in this region. The curve of [Si]:[Al] values is incapable to predict the experimental values in early stage of this region but matches pretty well in the later stage. At the "near equilibrium" region, $\Delta G_r > -25$ kJ mol^{-1}, the calculated [Si]:[Al] ratio decrease sharply, which is much lower than the experimental value. The discrepancy of [Si]:[Al] ratio between calculation and experiments may be due to the difference of secondary minerals formation controlled by different precipitation rates laws other than the "simple" rate law based on transition state theory.

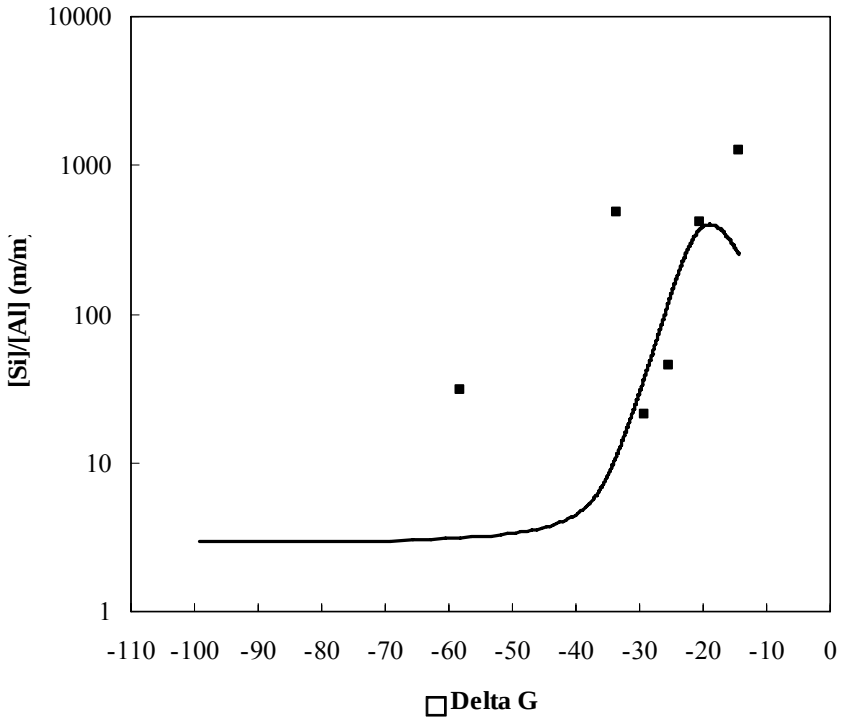

Figure 14. Calculated Evolution of [Si]:[Al] stoichiometry as a function of ΔG_r, compared to experimental data (as ΔG_r is a function of time, the sampling times are converted to ΔG_r values from simulation).

During our simulation, precipitation of boehmite occurs immediately as alkali-feldspar dissolves, but the occurrence of kaolinite and muscovite precipitation is postponed to 0.23 and 0.34 d, respectively. Boehmite, muscovite, and kaolinite precipitate continuously during the course of alkali-feldspar dissolution. The accumulated precipitation amounts of boehmite, kaolinite, and muscovite are 0 to 8.83×10^{-4}, 1.53×10^{-4}, and 1.61×10^{-5} moles, respectively during the course of 78 days (Fig. 15).

A sharp increase of boehmite (0 to 3.82 day, maximum rate as 4.9×10^{-10} mol/s), kaolinite (0.23 to 5.9 day, maximum rate as 7.6×10^{-11} mol/s), and muscovite (0.34 to 6.25 day, maximum rate as 5.74×10^{-12} mol/s) rates followed by a gradual decrease was observed (Figure 16), corresponding to saturation indices changing rapidly from being undersaturated to being supersaturated with the maximum values of 2.39 for boehmite, 4.67 for kaolinite, and 6.75 for muscovite, and then gradually reduce to 1.04 for boehmite, 3.05 for kaolinite, and 6.07 for muscovite (Figure 17b). However, the saturation indices of these secondary minerals do not match well with those calculated with solution chemistry data before 19 days' simulation. This may be also due to simple rate law (based on transition state theory) we used was incapable to simulate the real situation of secondary minerals precipitation or uncertainty of Al analysis for 1 and 9 day's samples, or both. There is little knowledge about secondary mineral precipitation rates, especially during the early stage of precipitation when crystal nucleation and growth involves (e.g., Hodson, 2003).

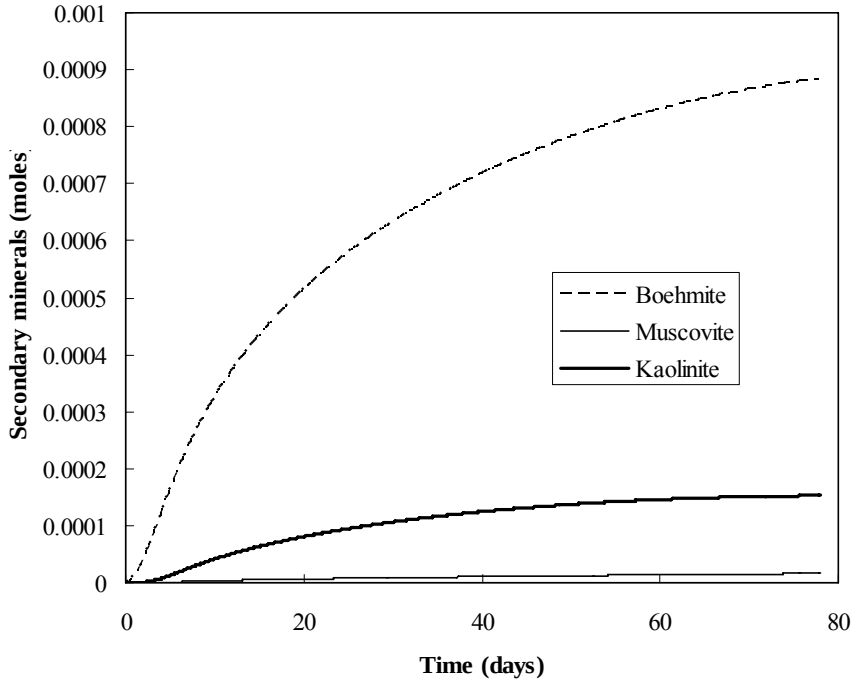

Figure 15. The calculated change in moles of secondary minerals with time during the course of alkali feldspar dissolution.

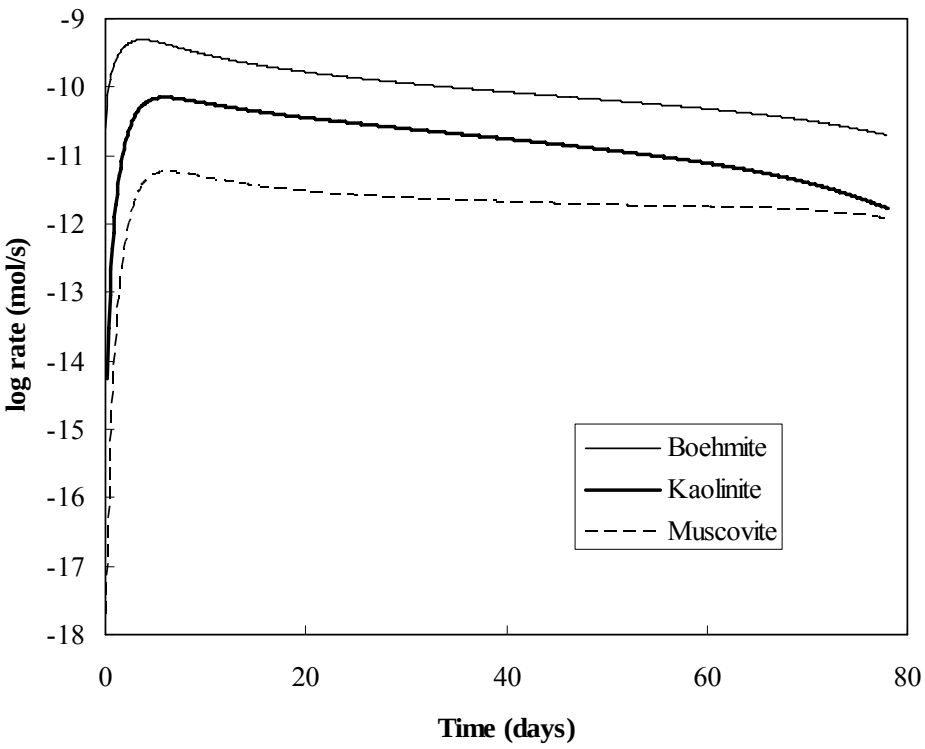

Figure 16. The calculated change in secondary mineral precipitation rates with time during the course of alkali feldspar dissolution.

With the equilibrium constants of mineral formation reactions and calculated total Na and K activities at 200 °C and 300 bars using the code PHREEQC, as well as in-situ pHs calculated in this study (Table 2), we are able to plot activity diagrams in the K_2O-Al_2O_3-SiO_2-H_2O-HCl (Figure 18) and Na_2O-Al_2O_3-SiO_2-H_2O-HCl (Figure 19) systems. In K_2O-Al_2O_3-SiO_2-H_2O-HCl activity-activity diagram, reaction path starts from boehmite field, through kaolinite field, to muscovite field, and approaching microcline field; In Na_2O-Al_2O_3-SiO_2-H_2O-HCl activity-activity diagram, the reaction path starts from boehmite field, but terminates in kaolinite field. Based on the phase diagrams, boehmite, kaolinite, and muscovite are the appropriate secondary minerals to be considered.

The calculated reaction paths of alkali-feldspar dissolution show a similar trend as those observed in experiments solution chemistry (Figs. 18 and 19). In Na_2O-Al_2O_3-SiO_2-H_2O-HCl system, the discrepancy of log activity of Na^+/H^+ in early stage may be due to the non-stoichiometric dissolution of feldspar, i.e., preferential release of Na^+, K^+ with respect to Si and/or initial release behavior which can be described by a rapid surface ion exchange reaction (Fung et al., 1980; Helgeson et al., 1984; Chou and Wollast, 1985). The reaction paths discrepancy in K_2O-Al_2O_3-SiO_2-H_2O-HCl system is not as much as in Na_2O-Al_2O_3-SiO_2-H_2O-HCl system, because (1) Ab dissolution is the dominant process and (2) the discrepancy of log activity of K^+/H^+ in early stage is masked due to high concentration of K (~0.2 M) in initial solution.

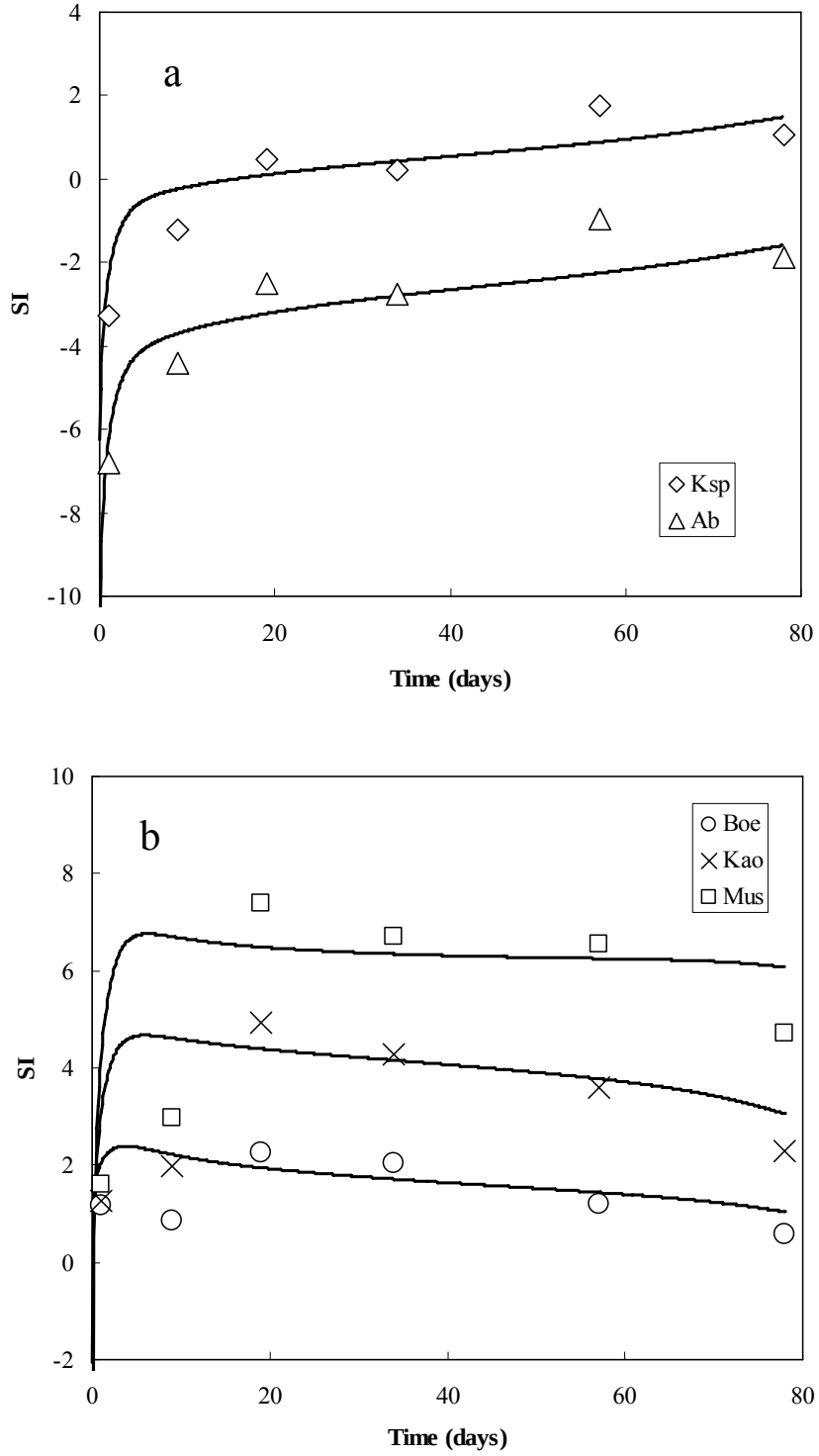

Figure 17. The calculated change in saturation indices evolution of (a) Ab and ksp and (b) boehmite (Boe), muscovite (Mus), and kaolinite (Kao) with experimental data with time during the course of alkali feldspar dissolution.

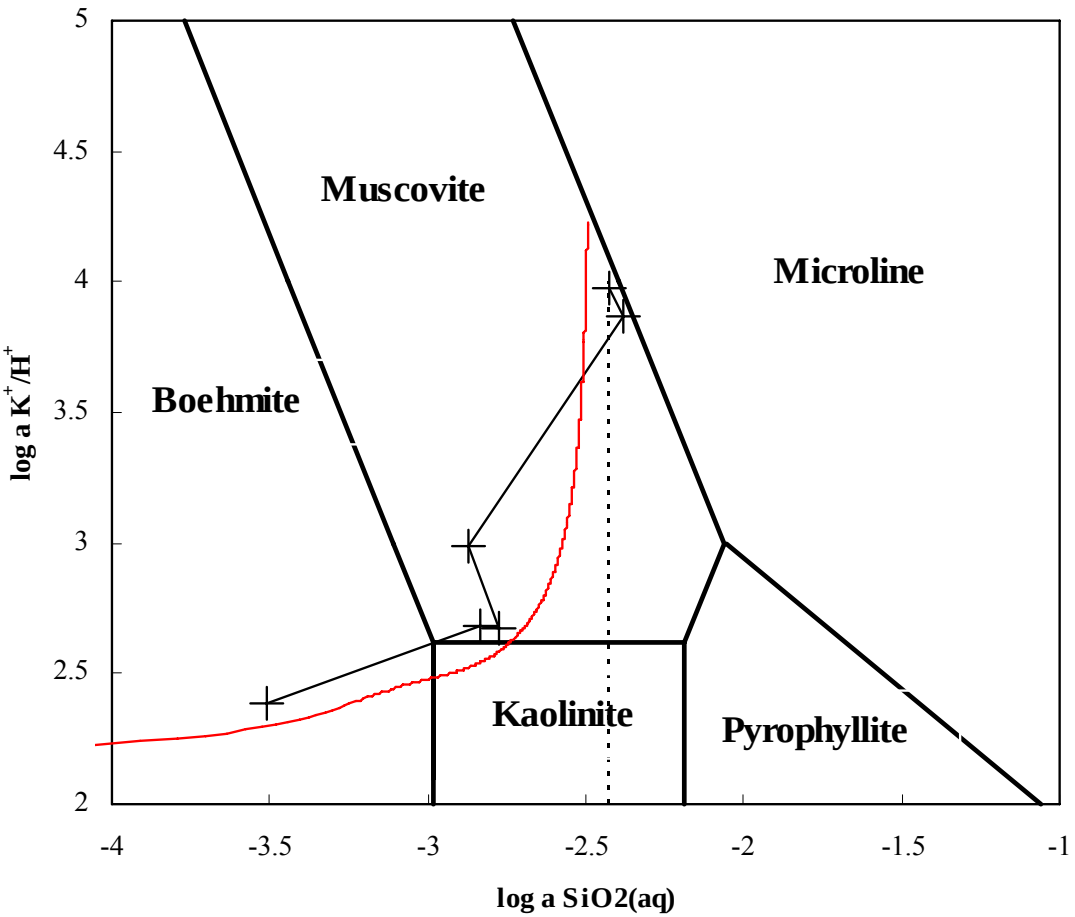

Figure 18. Activity diagram in the K_2O-Al_2O_3-SiO_2-H_2O-HCl system at 200°C and 300 bars. Fine dashed lines are quartz saturation line and boehmite boundary, respectively. Red line shows the reaction path of this simulation.

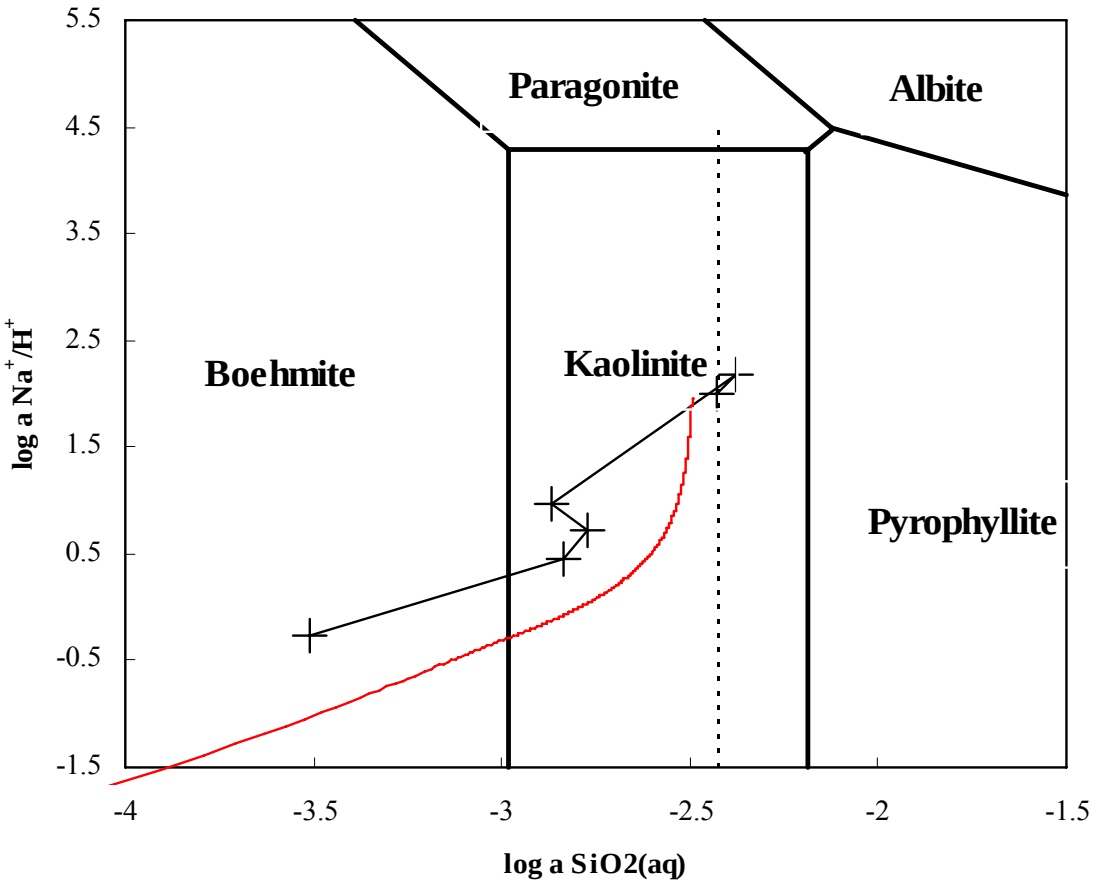

Figure 19. Activity diagram in the Na_2O-Al_2O_3-SiO_2-H_2O-HCl system at 200°C and 300 bars. Fine dashed lines are quartz saturation line and boehmite boundary, respectively. Red line shows the reaction path of this simulation.

5. Conclusions

This research project addresses some critical and urgent needs of the carbon sequestration program. The research program is built upon the PIs' substantial previous work in the field of water-gas-rock interactions, including some work in the carbon sequestration program. Hence, the funded work can be easily integrated with the NETL in-house research, and NETL-sponsored programs of field tests of injecting CO_2 into deep geological formations (Frio sandstone, Sleipner, and Weyburn projects), and mineral carbonation and brine sequestration programs (NETL, Los Alamos, Albany Research Center). Zhu has regular contact or formal/informal collaboration with many of the principal investigators in these programs.

Specially, during the second year of the three year project, we have accomplished the following:

- We successfully completed two batch type experiments and one flow-through experiment with Navajo sandstone and obtained time series solution chemistry data. An additional batch experiment was initiated with dawsonite. We also performed additional 5-day experiments at the same conditions as alkali-feldspar dissolution experiments with and without the presence of CO_2 performed in the first year to check the validation of the experiments and analysis. The products from these experiments were analyzed.

- We made significant progress on characterization of the reaction products by using SEM, TEM, and XPS.

- We conducted geochemical modeling work on interpretation of experimental results of alkali-feldspar dissolution experiments without the presence of CO_2.

- Two manuscripts are near completion.

Feldspar dissolution in natural waters often proceeds by consecutive reactions involving several steps to form the thermodynamically stable phase. The pioneering work to model feldspar dissolution as a system of coupled dissolution and precipitation was by Helgeson and coworkers (Helgeson, 1968a; Helgeson et al., 1969b). In their models, feldspar dissolution is treated as a kinetic process while equilibrium with respect to the secondary phases is assumed. The assumption of partial equilibrium for the formation of secondary phases during feldspar dissolution is greatly challenged by three lines of evidence, including field observation (Zhu et al., 2004; Zhu et al., 2006), experimental investigations (Nagy and Lasaga, 1993; Small, 1993; Price et al., 2005), and numerical modeling (Lasaga, 1984; Steefel and Van Capppellen, 1990; Lasaga et al., 1994; Lasaga, 1998), supporting that the formation of secondary minerals is a slow process once supersaturation with respect to a mineral is attained. Use of the assumption of partial equilibrium with respect to secondary phases in feldspar dissolution must be re-evaluated (Steefel and Van Capppellen, 1990). In the modeling study of Helgeson and coworkers (Helgeson, 1968a; Helgeson, 1969), kinetics of the secondary phases was not reported. As discussed in our modeling results, the kinetics of the secondary phases are coupled with feldspar dissolution, allowing kinetic simulation of precipitation and dissolution within the same environment.

The results show the inhibition of the feldspar dissolution followed by a large decrease in precipitation rates of boehmite, kaolinite and muscovite. These results can directly be compared with the field observations (Zhu et al., 2004; Zhu and Blum, 2005). Given the similar kinetics, kaolinite and muscovite precipitates while the enhanced feldspar dissolution is equally taken into account. The buildup of the Al or Si in the solutions is attributable to the assumed slow precipitation of kaolinite and muscovite, and simultaneously producing the overall similar pattern in the secondary minerals. A comparison of the simulated dissolution rates demonstrates that feldspar dissolution adequately reveals the influences of the kinetics of secondary minerals.

In summary, we have largely met or exceeded the milestones during the second year. We anticipate that the third year will be a more fruitful year as our graduate students are already trained and results from the second year are ready for interpretation and publication. Overall, our results will help to resolve one of the major outstanding scientific issues facing the carbon sequestration program: the rates of chemical reactions in geological formations. The results will benefit the program by introducing the development of numerical performance assessment models, which will reduce the costs of monitoring and design.

References Cited

Blum, A. and Stillings, L., 1995. Feldspar dissolution kinetics. In: Brantley, S. L. (Ed.), *Chemical Weathering Rates of Silicate Minerals*. Mineralogical Society of America, Washington DC.

Bradley, R. S., 2001. Many citations support global warming trend. *Science* **292**, 2011.

Burch, T. E., Nagy, K. L., and Lasaga, A. C., 1993. Free energy dependence of albite dissolution kinetics at 80° C and pH 8.8. *Chem. Geol.* **105**, 137-162.

Carey, J. W., Lichtner, P. C., Rosen, E. P., Ziock, H. J., and Guthrie, G. D. J., 2003. Geochemical mechanisms of serpentine and olivine carbonation. *Second annual conference on carbon sequestration*, Alexandria, Virginia.

Chou, L. and Wollast, R., 1985. Steady-state kinetics and dissolution mechanisms of albite. *American Journal of Science* **285**, 963-993.

Crowley, T. J., 2000. Causes of climate change over the past 1000 years. *Science* **289**, 270-277.

DOE, 1999. Carbon Sequestration Research and Development. U.S. Department of Energy.

Drever, J. I. and Clow, D. W., 1995. Weathering rates in catchments. In: Brantley, S. L. (Ed.), *Chemical Weathering Rates of Silicate Minerals*. Mineralogical Society of America.

Dulaney, A. R., 1989. The geochemistry of the N-aquifer system, Navajo and Hopi Indian Reservations, Northeastern Arizona. Master thesis, 209p, Northern Arizona University.

Fung, P., Bird, G. W., Melntyre, N. S., Sanipelli, G. G., and Lopata, V. J., 1980. Aspects of feldspar dissolution. *Nuclear Tech.* **51**, 188-196.

Gunter, W. D., Perkins, E. H., and Hutcheon, I., 2000. Aquifer disposal of acid gases: modelling of water-rock reactions for trapping of acid wastes. *Applied Geochemistry* **15**, 1085-1095.

Gunter, W. D., Wiwchar, B., and Perkins, E. H., 1997. Aquifer disposal of CO_2-rich greenhouse gases: extension of the time scale of experiment for CO2-sequestering reactions by geochemical modeling. *Mineralogy and Petrology* **59**, 121-140.

Hammerstad, T., 2000. Carbon dioxide storage prized. www.statoil.com.

Harshbarger, J. W., Repenning, C. A., and Irwin, J. H., 1957. Stratigraphy of the Uppermost Triassic and the Jurassic Rocks of the Navajo Country. U.S. Geological Survey Professional Paper 291.

Helgeson, H. C., 1968a. Evaluation of irreversible reactions in geochemical processes involving minerals and aqueous solutions-1. Thermodynamic relations. *Geochim. Cosmochim. Acta* **32**, 853-877.

Helgeson, H. C., 1968b. Evaluation of irreversible reactions in geochemical processes involving minerals and aqueous solutions-1. Thermodynamic relations. *Geochimica et Cosmochimica Acta* **32**, 853-877.

Helgeson, H. C., 1969. Thermodynamics of hydrothermal systems at elevated temperatures and pressures. . *Am. J. Sci.* **267**, 729-804.

Helgeson, H. C., 1979. Mass transfer among minerals and hydrothermal solutions. In: Barnes, H. L. (Ed.), *Geochemistry of Hydrothermal Ore Deposits*. John Wiley & Sons, New York.

Helgeson, H. C., Garrels, R. M., and Mackenzie, F. T., 1969a. Evaluation of irreversible reactions in geochemical processing involving minerals and aqueous solutions- II. Applications. *Geochimica et Cosmochimica Acta* **33**, 455-481.

Helgeson, H. C., Garrels, R. M., and Mackenzie, F. T., 1969b. Evaluation of irreversible reactions in geochemical processing involving minerals and aqueous solutions- II. Applications. *Geochim. Cosmochim. Acta* **33**, 455-481.

Helgeson, H. C. and Murphy, W. M., 1983. Calculation of mass transfer among minerals and aqueous solutions as a function of time and surface area in geochemical processes. I. computational approach. *Mathematical Geology* **15**, 109-130.

Helgeson, H. C., Murphy, W. M., and Aagaard, P., 1984. Thermodynamic and kinetic constraints on reaction rates among minerals and aqueous solutions II. Rate constants, effective surface area, and the hydrolysis of feldspar. *Geochim. Cosmochim. Acta* **48**, 2405-2432.

Hellmann, R. and Tisserand, D., 2006. Dissolution kinetics as a function of the Gibbs free energy of reaction: An experimental study based on albite feldspar *Geochim. Cosmochim. Acta* **70**, 364-383

Herzog, H., Drake, E., and Adams, E., 1997. Reuse, and Storage Technologies for Mitigating Global Climate Change.

Hodson, M. E., 2003. The influence of Fe-rich coatings on the dissolution of anorthite a pH 2.6. *Geochim. Cosmochim. Acta* **67**, 3355-3363.

Hovorka, S. D., Knox, P. R., Holtz, M. H., YEH, J. S., Fouad, K., and Sakurai, S., 2002. Sequestration pilot site in the Texas gulf coast, USA*GSA annual meeting & exposition abstracts with programs*, Denver, Colorado.

Johnson, J. W., Nitao, J. J., Steefel, C. I., and Knauss, K. G., 2002. Reactive transport modeling of geologic CO_2 sequestration. *GSA annual meeting & exposition abstracts with programs*, Denver, Colorado.

Johnson, J. W., Oelkers, E. H., and Helgeson, H. C., 1992. SUPCRT92 - A software package for calculating the standard molal thermodynamic properties of minerals, gases, aqueous species, and reactions from 1-bar to 5000-bar and 0°C to 1000°C. *Computers and Geosciences* **18**, 899-947.

Knauss, K. G., Steefel, C. I., Johnson, J. W., and Boram, L. H., 2002. Impact of CO_2, contaminant gas, aqueous fluid, and reservoir rock interactions on the geologic sequestration of CO_2*GSA annual meeting & exposition abstracts with programs*, Denver, Colorado.

Lasaga, A. C., 1984. Chemical kinetics of water-rock interactions. *J. Geophysical Res.* **89**, 4009-4025.

Lasaga, A. C., 1998. *Kinetic Theory in the Earth Sciences*. Princeton University Press, New York.

Lasaga, A. C., Soler, J. M., Ganor, J., Burch, T. E., and Nagy, K. L., 1994. Chemical Weathering Rate Laws and Global Geochemical Cycles. *Geochim. Cosmochim. Acta* **58**, 2361-2386.

Nagy, K. L. and Lasaga, A. C., 1993. Kinetics of simultaneous kaolinite and gibbsite precipitation. *Geochim. Cosmochim. Acta* **57**, 4329-4337.

NRC, 2003. Novel approaches to carbon management separation, capture, sequestration, and conversion to useful products workshop report. National Research council, Washington, DC.

Palandri, J. and Kharaka, Y., 2003. Ferric iron minerals as geologic traps for CO_2 sequestration: iron reduction using sulfur-bearing waste gas. *Chemical Geology*, In review.

Perkins, E. H., Gunter, W. D., Hutcheon, I., Shevalier, M., Durocher, K., and Emberley, S., 2002. Geochemical modelling and monitoring of CO_2 storage at the Weyburn site,

Saskatchewan, Canada. *GSA annual meeting & exposition abstracts with programs*, Denver, Colorado.

Price, J. R., Velbel, M. A., and Patino, L. C., 2005. Rates and time scales of clay-mineral formation by weathering in saprolitic regoliths of the southern Appalachians from geochemical mass balance. *Geological Society of America Bulletin* **117**, 783-794.

Seyfried, W. E., Jr., Janecky, D. R., and Berndt, M. E., 1987. Rocking autoclaves for hydrothermal experiments; II, The flexible reaction-cell system. In: Barnes, H. L. e. (Ed.), *Hydrothermal Experimental Techniques*. Wiley-Intescience.

Shock, E. L. and Helgeson, H. C., 1988. Calculation of the thermodynamic and transport properties of aqueous species at high pressures and temperatures: Correlation algorithms for ionic species and equation of state predictions to 5 kb and 1000° C. *Geochimica et Cosmochimica Acta* **52**, 2009-2036.

Shock, E. L., Helgeson, H. C., and Sverjensky, D. A., 1989. Calculations of the thermodynamic and transport properties of aqueous species at high pressures and temperatures: Standard partial molal properties of inorganic neutral species. *Geochimica et Cosmochimica Acta* **53**, 2157-2183.

Shock, E. L., Oelkers, E. H., Sverjensky, D. A., Johnson, J. W., and Helgeson, H. C., 1992. Calculation of thermodynamic and transport properties of aqueous species at high pressures and temperatures. Effective electrostatic radii, dissociation constants and standard partial molal properties to 1000°C and 5 kb. *J. Chem. Soc. London, Faraday Transactions* **88**, 803-826.

Small, J. S., 1993. Experimental Determination of the Rates of Precipitation of Authigenic Illite and Kaolinite in the Presence of Aqueous Oxalate and Comparison to the K/Ar Ages of Authigenic Illite in Reservoir Sandstones. *Clays and Clay Minerals* **41**, 191-208.

Steefel, C. I. and van Capppellen, P., 1990. A new approach to modeling water-rock interaction: The role of precursors, nucleation, and Oswald ripening. *Geochim. Cosmochim. Acta* **54**, 2657-2677.

Strazisar, B. R., Tan, H., Zhu, C., and Hedges, S. W., 2003. A reactive transport model of geochemical consequence upon injection of CO_2 into deep geological formations. *Journal of Contaminant Hydrology*, in review.

Sverjensky, D. A., Shock, E. L., and Helgeson, H. C., 1997. Prediction of the thermodynamic properties of aqueous metal complexes to 1000 degrees C and 5 kb. *Geochimica et Cosmochimica Acta* **61**, 1359-1412.

White, A. F., 1995. Chemical weathering of silicate minerals in soils. In: Brantley, S. L. (Ed.), *Chemical Weathering Rates of Silicate Minerals*. Mineralogical Society of America.

Xu, T., Apps, J. A., and Pruess, K., 2003. Numerical simulation to study mineral trapping for CO_2 disposal in deep aquifers. *Applied Geochemistry*, (in press).

Zhu, C., 2005. In situ Feldspar Dissolution Rates in an Aquifer. *Geochim. Cosmochim. Acta* **69**, 1435-1453.

Zhu, C., Blum, A., and Veblen, D., 2004. Feldspar dissolution rates and clay precipitation in the Navajo aquifer at Black Mesa, Arizona, USA. In: Wanty, R. B. and Seal, R. R. I. Eds. *Proceedings of the Eleventh International Symposium on Water-Rock Interaction WRI-11*. A.A. Balkema, Saratoga Springs, New York.

Zhu, C. and Blum, A. E., 2005. In situ silicate dissolution and precipitation rates in sandy aquifers. *Geological Society of America Abstr. with Programs*.

Zhu, C., Veblen, D. R., Blum, A. E., and Chipera, S. J., 2006. Naturally weathered feldspar surfaces in the Navajo Sandstone aquifer, Black Mesa, Arizona: Electron microscopic characterization. *Geochimica Et Cosmochimica Acta* **70**, 4600-4616.